A Comparison of Numerical and Analytical Predictions of the Tidal Stream Power Resource of Massachusetts, USA

Geoffrey W. Cowles[a], Aradea R. Hakim[a], James H. Churchill[b]

[a] *Dept. of Fisheries Oceanography*
University of Massachusetts Dartmouth
New Bedford, MA 02744, USA

[b] *Dept. of Physical Oceanography*
Woods Hole Oceanographic Institution
Woods Hole, MA 02543, USA

Abstract

The coastal waters of Massachusetts, USA encompass tidal phenomena that generate flows of sufficient magnitude for commercially viable power extraction. We examine the tidal power resource of the Massachusetts coastal region with two high-resolution hydrodynamic tidal models: a regional model encompassing the coastal waters of southeastern New England and a local domain model of Cape Cod Canal. Both models have been subject to comprehensive skill assessment using available surface elevation and ADCP measurements. Based on the model results, we identify five high-energy sites (Cape Cod Canal, Muskeget Channel, Quicks Hole, Robinson Hole and Woods Hole) for evaluation of the maximum extractable tidal power. The power extraction at these sites is modeled using linear momentum actuator disk theory applied to a cross-channel array of turbines. Of the sites evaluated, Muskeget Channel has the greatest resource, with an estimated maximum extractable power of 24 MW. The estimated total power available from all five sites is 44 MW. These estimates agree within 21% with predictions from analytical approaches at all sites. Potential applications for the models include: providing developers with an initial assessment of the resource, guiding observation programs for further study of the resource, and facilitating optimization of turbine array design.

Keywords: tidal power, FVCOM, Cape Cod Canal, Muskeget Channel

Highlights:
- A three dimensional barotropic tidal model for Massachusetts has been validated
- LMADT theory is used to evaluate the theoretical tidal stream power resource
- Results compared with values derived from accepted analytical approaches of Garrett & Cummins
- A maximum extractable power of 44 MW is available from five high energy sites

Email address: gcowles@umassd.edu (Geoffrey W. Cowles)

Preprint submitted to Renewable Energy *April 25, 2017*

1. Introduction

The tidal range within the coastal waters of Massachusetts may be characterized as moderate, with the amplitude of the dominant M_2 constituent ranging from 0.4 to 1.5 m [1,2,3]. Nevertheless, strong tidal velocities ($> 1.5\ \mathrm{m\,s^{-1}}$) have been observed in the Massachusetts coastal zone [3,4]. Observational and modeling studies [3,4,5,6,7] have revealed two dominant mechanisms responsible for these strong tidal flows. One is the complex interference of two regional-scale tidal waves, and the other is generation of a rapid flow through a narrow passageway by differing tidal regimes bordering the passageway.

As first described by [4], the interference phenomenon is generated by two tidal waves, one which propagates northward from the shelf break south of New England and the other which first passes through the Gulf of Maine before turning south into Nantucket Sound. The result is a rapid variation of tidal phase over a region stretching from Nantucket Shoals to Vineyard Sound (Fig. 1. upper panel). Although the tidal range in this region is small ($<$ 0.5 m), the resulting tidal currents can be quite strong ($>1.5\ \mathrm{m\,s^{-1}}$). The interference zone includes Muskeget Channel, a well-defined feature of roughly 10 x 0.6 km (as delineated by the 15-m isobath) situated between Martha's Vineyard and Nantucket (Fig. 1, lower panel), as well as Vineyard Sound, which separates Martha's Vineyard from the Elizabeth Island Chain (Fig. 1, center panel).

Strong tidal flows generated by elevation differences of separate tidal systems, the second mechanism cited above, appear in the passageways connecting Buzzards Bay with Vineyard Sound. The tide in Buzzards Bay can be described as a standing wave that propagates directly from the open ocean to the southwest [8]. It is separated from the tidal regime of Vineyard Sound by the Elizabeth Island chain (Fig. 1, center panel). The tidal phase and amplitude difference between Buzzards Bay and Vineyard Sound generates strong currents in the four channels (or holes) of the Elizabeth Island chain. Three of these passageways, Woods Hole, Robinson Hole and Canipitsit Channel are less than 0.5 km wide, whereas the fourth, Quicks Hole, is $\sim$1.4 km in width. Differing tidal regimes also produce strong tidal flows through Cape Cod Canal, an artificial waterway approximately 12.5 km long, 0.2 km wide and 10-23.5 m deep [9] that links Cape Cod Bay and Buzzards Bay (Fig. 1, upper panel). The tidal forcing of the canal is highly asymmetric, with the tidal range at the Cape Cod Bay entrance exceeding that of Buzzards Bay by a factor of 3 and the time of high tide lagging by more than 3 h.

Over the past decade several marine renewable energy companies have expressed interest in tapping the tidal stream power potential of Massachusetts' coastal waters. Four preliminary permits and one pilot permit have been filed with the Federal Energy Regulatory Commission (FERC) at three sites: Vineyard Sound, Muskeget Channel, and Cape Cod Canal (Fig. 1).

An early assessment of the tidal power resource of Massachusetts' waters, employing available velocity measurements, was formulated by [10] of the Electrical Power Research Institute (EPRI). They identified four sites, Cape Cod Canal, Muskeget Channel, Woods Hole, and Blynman Canal (northern Massachusetts), with annual mean power densities in excess of 0.7 $\mathrm{kW\,m^{-2}}$. Using nearby single point velocity measurements, Hagerman and Bedard estimated the tidal power resource at each site by computing an annual power density and applying this to the cross sectional area of a representative transect at each site. The time-averaged total power available at the four sites was estimated to be 33.8 MW. The estimated extractable power, determined by applying a significant impact factor of 15%, of the four sites totaled 5.1 MW.

A second assessment of the Massachusetts coastal zone tidal power resource was formulated by [11] as part of a national geodatabase of tidal energy for the entire United States. They employed a hydrostatic, primitive-equation ocean model, ROMS, set up on grid with a horizontal mesh scale of approximately 350 m. They established three criteria for tidal power hotspots: (1) annual mean power density exceeding 0.5 $\mathrm{kW\,m^{-2}}$, (2) horizontal area greater than 0.5 $\mathrm{km^2}$, and (3) depth greater than 5 m. Four hotspots were identified in Massachusetts' coastal waters: Nantucket Shoals, Muskeget Channel, and the northern and southern extents of Vineyard Sound (Fig. 1). Using the analytical formulation of [12], they estimated the theoretical tidal power resource of the Massachusetts coastal zone to be 45 MW.

While the above studies have provided useful initial assessments of the tidal power resource in the Massachusetts coastal zone, their findings must be viewed with caution, as they are based on a limited number of observations [10] or on results of a low-resolution numerical model [11]. In particular, use of coarse-mesh hydrodynamic models limits the skill of assessing tidal power over areas of strong currents, such as in constricted channels and near headlands [13,14,15]. For such areas, higher-resolution, local-domain models are required to provide a detailed assessment of the tidal power resource. Furthermore, [16] demonstrated that because velocities at high-energy sites tend to exhibit significant vertical shear, models with high vertical resolution are required to guide the vertical turbine placement for maximum power extraction. To ensure that the model-derived characterization of the tidal resource is accurate, the model needs to be substantially validated with observations in the vicinity of the tidal resource to be evaluated.

While evaluating the details of a tidal power resource clearly requires a high-resolution, and validated, hydrodynamic model, simple analytical formulae derived by Garrett and Cummins ([12,17]; hereafter GC05 and GC07) have proven useful in producing estimates of maximum extractable power from a constrained tidal flow. The estimates are achieved using properties of the flow (i.e., maximum volume flux through a channel) and the sea surface elevation field (i.e., difference in tidal head on either side of a channel) of the area from which tidal power is to be extracted, and entail far less computational effort than required for estimating maximum extractable power with high-resolution numerical models. The formulae are applicable to two different turbine arrangements relative to flow boundaries. GC05 applies to the scenario in which a "fence" of turbines extends across a full channel width, whereas CC07 is derived for the more complicated scenario in which a turbine fence occupies only a portion of the channel. A number of investigators (e.g. [18,19,20]) have tested the GC05 and GC07 formulae by comparing their results with estimates of maximum extractable tidal power computed by representing the effects of turbines in high-resolution hydrodynamic models. In all published cases, the numerically-derived estimates closely agree (generally to within 30%) with those determined from the formulae of GC05 and GC07, establishing the utility of these formulae for determining initial estimates of maximum extractable tidal power. To our knowledge, however, all comparisons have been carried out for environments of relatively high tidal power potential (with estimates of maximum extractable power generally > 400 MW), so the accuracy of the GC05 and GC07 formulae in estimating maximum extractable tidal power for environments with modestly strong tidal power potential, as found in the Massachusetts coastal zone, is currently unknown.

Our study was carried out with a principal goal of generating a detailed assessment of the tidal power resource of the Massachusetts coastal zone. Using a high-resolution, three-dimensional barotropic tidal model, we estimated the maximum theoretical tidal power at sites off the Massachusetts coast. The scheme entailed modeling power extraction at designated sites using linear momentum actuator disk theory applied to a cross-channel turbine array, and increasing the level of extraction until peak power removal was achieved. The model was also used to evaluate the impact of tidal power extraction on volume flux, taken as a metric for the effect of power extraction on the local environment. As detailed below, the model was extensively tested using observations of tidal velocities and sea surface elevations distributed throughout the model domain.

A second goal of our study was to compare the power resource estimates determined as described above with estimates obtained from the analytical formulae of GC05 and GC07, providing tests of these formulae for environments with modest tidal power potential.

2. Approach

2.1. Ocean Model

Our study employs a hydrostatic, primitive-equation (HPE) model, known as the Finite Volume Community Ocean Model (FVCOM; [21,22]), as the modeling tool. In FVCOM, the HPEs are discretized on an unstructured horizontal grid and a terrain-following vertical grid. An explicit mode splitting approach is used to advance the model equations [23]. The spatial fluxes of momentum are discretized using a second-order accurate finite-volume method [24]. Exact conservation of scalar quantities (e.g., temperature, salinity, turbulence) is achieved by combining a scalar flux formulation with a vertical velocity adjustment. The model is parallelized using an efficient single-program-multiple-data approach [25] that scales efficiently on modern distributed memory computing systems. Domain decomposition for the parallel model is performed using the METIS graph partitioning libraries [26]. Interprocessor communication is programmed using the Message Passing Interface standard using a non-blocking approach. The horizontal eddy diffusivity is parameterized using a Smagorinsky formulation [27]. The General Ocean Turbulence Model (GOTM, [28]) is coupled to FVCOM to compute the vertical eddy viscosity and diffusivity. The two-equation, k-ϵ eddy viscosity model was selected for the present work.

The barotropic tides of the Massachusetts coastal zone are examined using two FVCOM-based models. One, the Massachusetts Tidal Model (MTM), is regional and covers the entirety of the Massachusetts coastal zone. The second, a local-domain model, is employed for the study of the Cape Cod Canal. Referred to as the C^3M model, this is nested within MTM using a one-way approach. These models are described in detail in the following subsections.

2.1.1. Massachusetts Tidal Model (MTM)

The MTM encompasses all of the Massachusetts coastal zone as well as the coastal waters off of Rhode Island and New York (Fig. 2). The Massachusetts coastal boundary is derived from a high-resolution (1/2 $''$) Massachusetts coastline product developed by the Massachusetts Office of Coastal Zone Management. The model bathymetry is interpolated from a composite dataset. The majority of the model domain is covered by the 3-arc-second Gulf of Maine bathymetry product [29] and the 1/3 $''$ Nantucket Inundation Digital Elevation Model (NOAA: [30]). Regional surveys are used to refine the model bathymetry in specific areas of interest. These include a 1-m resolution SWATH bathymetry survey in Muskeget Channel [31] and a directed sounding survey of the Cape Cod Canal [9]. The MTM domain is tessellated using a sequence of grids for the purpose of evaluating the dependence of the flow solution on the model resolution. The finest mesh, MTM-1, contains 228K horizontal grid elements, with a resolution ranging from 25 m along the coast and in areas of interest to 10 km at the open boundary. The MTM vertical coordinate is discretized using ten equally spaced sigma-layers. The model is driven by six tidal constituents ($\mathrm{M_2, S_2, N_2, K_1, O_1, M_4}$) at the open boundary. The model forcing does not include buoyancy (heat flux, precipitation, and river flux) or wind forcing. Free-slip conditions are applied along the lateral boundaries.

Values for the phases and amplitudes of the six tidal constituents have been developed using the following incremental approach. Initial values for the diurnal and semidiurnal components are interpolated from the FVCOM Gulf of Maine regional tidal model [3]. Initial values for the $\mathrm{M_4}$ component on the open boundary are derived from the Tidal Model Driver based on the Oregon State University Tidal Inversion Software (OTIS, [32]). The constituents on the open boundary are then tuned over a sequence of model runs to minimize the discrepancy between model-computed harmonics and observed harmonics in the interior of the domain. Formulation of the spatially-varying bottom roughness, z_0, follows a depth-dependent criteria originally formulated by [3]:

$$z_0 = \begin{cases} 3\times10^{-3} & \text{for } h \le 40 \\ 3\times10^{-3}e^{-(h-40)/8.82} & \text{for } 40 < h \le 70 \\ 1\times10^{-4}e^{-(h-70)/13.03} & \text{for } 70 < h \le 100 \\ 1\times10^{-5} & \text{for } h > 100 \end{cases} \tag{1}$$

where h is the static water depth in meters. The fine-grid model (MTM-1) is integrated with a 2.5 s time step and requires approximately 24 core-hours on an Intel Haswell system to advance one $\mathrm{M_2}$ period. The model is integrated forward for 60 d of simulation time in order to provide a sufficient duration for stable computation of the six primary regional constituents of tidal elevation and velocity.

2.1.2. Cape Cod Canal Model $\mathrm{C^3M}$

The $\mathrm{C^3M}$ domain, used for the study of tides in the Cape Cod Canal, includes the southwestern portion of Cape Cod Bay, the Cape Cod Canal proper, and the northeastern portion of Buzzards Bay (Fig. 2). The $\mathrm{C^3M}$ mesh resolution varies from 10 m within the Canal to 500 m at the open boundaries. The mesh contains 43,682 horizontal grid elements and 10 equally spaced vertical sigma layers. The $\mathrm{C^3M}$ bathymetry is derived from a recent survey of the

Canal conducted by the Army Corp of Engineers [9]. The model is barotropic and is forced only by sea surface elevation based on the six principal constituents ($M_2, S_2, N_2, K_1, O_1, M_4$) at the open boundaries. On the western open boundary, the harmonics are derived using pressure data from the NOAA Current Measurement Interface for the Study of Tides (CMIST; [33]) station C0D0906, located near Abiels Ledge in Buzzards Bay. The length of this open boundary is short (∼1300 m) and of relatively constant depth which enables a single observation at a fixed point to be used to establish the elevation along the entire boundary. On the eastern open boundary in Cape Cod Bay the surface elevation forcing is interpolated from the regional MTM model described above. A study of the influence of bottom roughness in the C^3M model found that a uniform value of $z_0 = 0.01$ m results in the best agreement of velocity and surface elevation with the available measurements along the canal. Assuming that the roughness scales only with grain size, this value of z_0 corresponds to cobbles in the Wentworth scale. Although it is likely that bedforms may be present in the canal due to the high flow speeds, this grain size is within the range of surficial sediment distribution observed in the region [34]. The C^3M is integrated using a time step of 0.4 s, which requires 12 core-hours on an Intel Haswell system to advance the model one M_2 cycle. To reach steady values for the harmonic decomposition of the six constituents, the model is run for 60 d of simulation time.

2.2. Skill Assessment and Model Validation

2.2.1. Tidal Elevation

The model skill in simulating sea surface elevation is evaluated using a tidal harmonics database derived from several sources: the National Ocean Service [35], the U.S. Geological Survey tidal atlas [1], the Nantucket Shoals Flux Experiment [2,6], the Coupled Boundary Layers Air-Sea Transfer experiment [36], the Coastal Mixing and Optics Experiment [37], the CMIST database [33] and a recent study of Muskeget Channel [38]. Tidal harmonics are computed from the water level time series using the MATLAB routine T-Tide [39]. The resulting database contains harmonics at 73 unique locations within the model domain. These tidal harmonics, and those derived from the model simulations (described above), are used to construct year-long time series of tidal elevation. Following recent recommendations for skill assessment methods for tidal resource modeling [15], model skill is evaluated as the root mean square error (RMSE) between the observed and model time series.

The mean and maximum RMSE of the annual time series of sea surface elevation over all 73 stations is 5.6 cm and 12.0 cm, respectively (Fig. 3). A geographic pattern of model error is revealed by the distribution of binned RMSE values. The lowest error bin (RMSE $\leq$ 3 cm) is populated primarily by stations in deeper water ($>$ 25 m depth), including stations near the open boundary. The majority of stations in the second error bin ($3 <$ RMSE ≤ 6 cm) are in shallow, nearshore water. The third error bin ($6 <$ RMSE ≤ 9 cm) is comprised mainly of shoreside stations. Shoreside stations are also the dominant contributor to the largest error bin ($9 <$ RMSE ≤ 12 cm). Three of the seven stations in the bin are found near the line of rapidly varying phase that extends from Woods Hole across Martha's Vineyard to Nantucket (Fig. 1). The mean RMSE for the M_2 sea surface elevation amplitude over the 73 stations is 2.86 cm, which is 4% of the mean M_2 amplitude of 68.7 cm. The RMSE for the M_2 phase is 9.4° or 19.5 min. Phase and amplitude for the six primary constituents of the observed and model-computed sea surface elevation at the 73 stations are included in online Supplementary Material (S.1-S.2).

2.2.2. Tidal Ellipses and Power Density at Fixed ADCP Locations

The model skill in simulating currents and power density is evaluated with flow velocity measurements obtained from both fixed and shipboard current meters. The fixed current meter data are from the CMIST program [33] and include currents measured by 11 bottom-mounted, upward-looking ADCPs deployed within the MTM domain during 2009 for durations of 1 to 3 mths. These velocity data were archived at 6-min intervals and extend vertically in 1.0-m bins from 2.5 m above bottom to $\sim$2 m below the surface. In addition, the CMIST data include velocities from a sideward-looking ADCP deployed from the south pier of the Cape Cod Canal railroad bridge from 3 June 2009 to 21 July 2009. These data have a horizontal resolution of 4 m. The CMIST records carry the prefix COD09 in the online database, but will be designated here with the prefix CMIST-.

Assessment of the model skill in reproducing the orientation, ellipticity, and magnitude of the tidal current is performed using the vertically averaged velocity records from the fixed upward-looking CMIST ADCPs. Tidal ellipses of the vertically averaged flow are derived from these velocity records, and from the vertically averaged model velocities at each CMIST site, by first determining the six principal tidal constituents ($M_2, S_2, N_2, K_1, O_1, M_4$) using T-Tide and then using these constituents to construct annual modeled and measured tidal time series. These annual time series are also used to evaluate the model skill in estimating the vertically averaged power density.

The model very closely reproduces the orientation, eccentricity, and magnitude of the vertically averaged tidal flow at the 12 CMIST sites (Fig. 4). However, it should be noted that the orientation of the observed tidal ellipses in the Cape Cod Canal have been adjusted to be parallel to the canal centerline. The measured tidal velocities at two of the three upward-looking ADCP stations in the canal had major axis orientation deviating by more than 20° from the canal centerline. These orientations also shifted during the observation period indicating possible problems with the compass and/or movement of the tripod.

Ellipticity of the modeled and measured tidal current is small at all CMIST sites. Ellipticities of the model-computed tidal velocities have a mean value of 0.024, with a minimum of 0.002 occurring in the canal at CMIST-2 and a maximum value of 0.11 at CMIST-12. The observed velocities have a mean ellipticity of 0.022 with a minimum value of 0.002 at CMIST-3 in the canal and maximum of 0.090 at CMIST-12. CMIST-12, in the Woods Hole channel, is the only CMIST station with ellipticity greater than 0.04 in either the model-computed or observed records. This is due to a considerable difference in the direction of ebb and flood flows, which is associated with separation of the flood tide (eastward) flow on the downstream side of the sharp bend in the Woods Hole channel.

For the skill assessment of vertical structure of the model-computed flows, we focus on comparisons of kinetic power density rather than velocity, as this metric is a better indicator of the ability of the model to capture the theoretical in-stream tidal power resource. As the kinetic power density scales with the cube of the current speed, the power density errors are correspondingly amplified with respect to velocity errors. Kinetic power densities are determined from the six principal tidal constituents, as described above, using the modeled and measured tidal velocity time series at the CMIST sites. To demonstrate the model skill in estimating the power density, we present the power density RMSE, the annual mean value of power density, and a relative average error using a metric defined by [40] as

$$WM = 1 - \frac{\Sigma \left| P_{model} - P_{obs} \right|^2}{\Sigma \left(\left| P_{model} - \bar{P}_{obs} \right| + \left| P_{obs} - \bar{P}_{obs} \right| \right)^2} \tag{2}$$

where P represents kinetic power density and the overbar denotes averaging over the dataset. For comparison of vertically averaged velocities at a CMIST station the overbar represents averaging over the annual time series. The parameter WM (Willmott) ranges from 0 (complete disagreement) to 1 (perfect agreement).

Comparison of model- and data-derived vertically averaged power densities at the 11 upward looking ADCP sites gives Willmott scores of 0.89 to 0.99 and RMSE values of 0.03 to 0.48 $\mathrm{kW\,m^{-2}}$ (Table 1). The maximum annual mean power density occurs at CMIST-2 (Sagamore Bridge) based on both model-computed and observed time series (Table 1).

The vertical profiles of annual mean power density (Fig. 5) reveal some interesting spatial differences in the model skill. At the sites of the upward looking ADCPs inside the Cape Cod Canal (CMIST-1 to CMIST-3) the model-observation agreement of power density shear and magnitude is very good. At the site of the horizontal ADCP (CMIST-4) in the canal, the maximum kinetic power density compares well with observation but the model-computed values near the edges of the canal exceed the measurements. At CMIST-5 outside the west canal entrance, the model-computed power densities are underpredicted at all depths. The model-derived power density profile at CMIST-6 is in good agreement with the observed profile, through with a slightly greater shear. CMIST-6, in the upper portion of Buzzards Bay, is a low energy site with peak annual mean power density of 0.15 $\mathrm{kW\,m^{-2}}$. The model skill at the three stations in Woods Hole (CMIST-10 to CMIST-12) are the lowest of the set. The model overpredicts the power at both the west (CMIST-10) and east (CMIST-12) entrances. In the strait where the energy is highest (CMIST-11), the vertical average of power density is in good agreement but the model fails to predict the significant shear at the site. At the remaining channels through the Elizabeth Islands (CMIST-13 to CMIST-15), the model-computed and observed values of kinetic power density are in good agreement.

2.2.3. Power Density along Transects

Shipboard current data was acquired from a vessel-mounted ADCP during surveys conducted in Muskeget Channel on 29 August 2008 and 25 June 2009 [38]. Surveys from both years coincided with stronger than average spring tides. Four transects were surveyed at approximately 1-h intervals over a tidal cycle (Fig 1, lower panel). On average, the ship required 6.5 min moving at 3.5 kts for each transit across the Channel.

A specific model time for each transect must be chosen for the skill assessment, as the model velocity field is archived at a 10 min interval. For each transect, we use the model field from a time closest to the measurement time at the midpoint of the transect. The model and ADCP velocity data of each transect are interpolated onto a common grid with a resolution of 10-m in the along-transect direction and 1-m in the vertical. From the gridded data, we compare the kinetic power density profiles at several stations along the transect, and compute RMSE and Willmott scores for the kinetic power density over the transect. In computing the transect Willmott score, the overbar in equation 2 represents a spatial average over the discrete locations in the transect. Total observed and model-computed kinetic power through the transects are also presented during peak ebb and flood.

Willmott scores for the ADCP transects (T6-T9) in Muskeget Channel (see Fig. 1, lower panel for locations) range from 0.92 to 0.98, while the RMSE of power density over these transects ranges from 0.08 $\mathrm{kW\,m^{-2}}$ (T9, flood) to 0.72 $\mathrm{kW\,m^{-2}}$ (T7, ebb) (Table 2). Differences in the modeled and observed total power in the transect range from 2% to 25% of the observed power (Table 2). There is notable tidal phase asymmetry of flow in the southern transects (T7-T9) with dominance of the ebb (southward) flow. Within T8, for example, the peak power density during ebb is more than twice that during flood (Fig. 6). In addition, there is a significant flood-ebb difference in the spatial structure of the power density. During flood, the core of maximum power is centered towards the east side of the channel, while during ebb it resides towards the west side of the channel. There is also significant vertical shear in the flow. The model captures the shear in the power density profile very well in areas of high power and less so outside these regions (Fig. 6).

2.3. Resource Quantification

2.3.1. Power Density

A key metric of the extractable power potential is the kinetic power density. Annual mean kinetic power density, P_A, is computed at each element in both the MTM and C^{3}M domains based on the vertical average of the power density in each layer,

$$P_A = \overline{\frac{\rho}{2N}\sum_{k=1}^{N}\left(\sqrt{u_k^2+v_k^2}\right)^3} \tag{3}$$

where $\rho = 1025$ kg m^{-3} is the density of the water, (u_k,v_k) are the horizontal velocities in layer k reconstructed from the harmonic constituents for one year at ten minute intervals, N=10 is the number of vertical layers, and the overbar indicates an annual mean. For consistency, this metric is computed as the vertical average of kinetic power density rather than the kinetic power density of the vertically averaged velocity, although the difference between these quantities is only a few percent. An average over the water column is used in place of a kinetic power density determined from surface or near-bottom velocities as turbines are likely to be placed away from both the surface- and bottom-boundary layer, making the vertically averaged power a suitable indicator of available resource.

The annual mean kinetic power density is used to select the locations for evaluation of the theoretical in-stream power potential. In prior studies, various power density thresholds have been employed for identifying promising locations for tidal power extraction. These include 0.25 kW m^{-2} [41], 0.5 kW m^{-2} [11], 0.7 kW m^{-2} [10] and 1.0 kW m^{-2} recommended by the Northwest National Marine Renewable Energy Center ([42,43]). For this work, we use the intermediate threshold value of 0.7 kW m^{-2}. For flows with limited tidal asymmetry, this corresponds to peak speeds of 1.5 m s^{-1} and instantaneous speeds exceeding a turbine cut-in value of 1 m s^{-1} for more than half of the tide cycle [44].

2.3.2. *Theoretical Power*

The theoretical resource within a designated channel is evaluated by placing a row of turbines across the channel, an approach used for investigations of the tidal power resource in British Columbia [18], Minas Passage [19] and the Pentland Firth [20]. Here, a row of turbines is referred to as a fence to be consistent with the terminology of previous theoretical studies [12,17]. For sites with well defined lateral land boundaries, a full channel-width fence is used. In this case, the flow is forced to pass across the fence. For sites where lateral boundaries are poorly defined, a partial fence is used. For this case, the row of turbines spans a channel feature defined by bathymetric contours and the water is able to partially pass around the fence. In all cases, there are no gaps in the fence and momentum is extracted from the entire water column. The mesh is modified locally so that mesh elements align with the strip along which the turbines are placed. The advantage of using a fence is that it avoids the need to properly model the interactions between individual turbines that occur in a staggered array. It should be noted that this provides an estimate of the maximum power potential of a site.

Power extraction is simulated by adding a momentum sink term formulated using the linear momentum actuator disk approach of [45] (see [46] for details on the term's implementation in FVCOM). The only input parameter required to model the power extraction is the turbine thrust coefficient, C_T. Preliminary investigations indicated that the difference in maximum power achieved by varying C_T along the fence as opposed to using a spatially-constant C_T is negligible. Hence, in this work a constant C_T is used along the entire fence. The value of C_T is increased to the point of maximum power extraction. This approach provides an upper bound on the extractable power. The practical extractable power depends on the characteristics of the specific technology installed (e.g. thrust coefficient, cut-in speed) as well as site specific exclusion constraints such as the need to maintain a navigation channel.

In addition to estimation of the theoretical tidal stream resource that can be extracted, we examine the impact of power extraction on the volume flux. Changes in volume flux is an important impact metric as it can be viewed as a proxy for potential alterations in flushing and transport, and can be useful in setting thresholds for acceptable levels of power extraction [19,47].

The theoretical resource is computed for forcing by only the M_2 tide only as well as by all six major constituents. For M_2 forcing, the model is run for four days, and mean power and other metrics are determined from the last tidal cycle. For runs with all constituents, the model is run for 60 d, and harmonic analysis is used to construct an annual time series. Since the M_2-forced simulations run rapidly, these are used to generate power curves and explore the relationship between power extraction and volume flux. Runs with the six major constituents are executed for C_T values near those which produced peak power for M_2 only and are used only to produce the peak annual mean power at a given site.

2.3.3. Analytical Approaches

The model-computed maximum tidal stream power is compared with accepted analytical formulations for maximal power in a 1-D channel extracted with a full (GC05) and partial (GC07) fence. The formula for a full fence, GC05, is:

$$P_{FF} = \gamma \rho g a Q_o \tag{4}$$

where P_{FF} is the time-average power, a is the maximum head difference from one of the channel to the other, Q_o is the maximum volume flux through the channel with no power extraction, g is the gravitational acceleration, ρ is the fluid density, and γ is a coefficient related to the the relative importance of bottom friction in dynamic balance of the channel. Values of γ range from 0.196 to 0.24, with the larger value representing a channel with no bottom friction (see Fig. 4 in GC05). The GC05 model assumes that the tidal range in the channel is small compared to the depth, the bottom friction can be parameterized with a constant drag coefficient, and the tidal head difference, a, is not influenced by energy extraction. The GC05 formulation provides a relatively simple means of estimating the maximum power resource in a channel, and allows for quick identification of areas where the tidal resource may be worthy of more intensive study. However, the results of the GC05 formulation should be viewed cautiously as not all of its assumptions may be valid in a realistic setting.

As noted above, a partial fence is employed in this work for sites is which the area of power extraction is not a confined channel. For such sites, flow is able to pass around the turbine array. In the absence of lateral walls and free surface effects, maximum achievable power is established by the Betz limit [48]. However, for many sites the influence of lateral boundaries cannot be neglected. This was addressed by GC07, who derived the following expression for maximum power for a partial fence:

$$P_{PF} = \frac{1}{2}\left(1 - r_b\right)^{-2} \eta A_T \rho u_0^3 \tag{5}$$

The quantity u_0 is the average velocity magnitude of the natural flow (without power extraction) over a tidal cycle, $\eta = 16/27$ is Betz's coefficient, and $r_b = A_T/A_c$ is the channel blockage ratio where A_T is the turbine cross sectional area and A_c is the total channel area.

The flow properties needed to compute the above power estimates (e.g. a, Q_o,u_0) are derived from model results under M_2-only forcing. Computation of the head difference, a, in a manner consistent with the assumption of GC05 (that a is unaffected by extraction of power from the channel) poses a challenge. This is noted by [20], who conformed with the GC05 assumption by evaluating a from the tidal head at two points where effects of the turbine fence has been dissipated. To estimate the parameter γ in the GC05 formula for each site we use the model output to compute the phase lag of the discharge at the position of the fence with respect to the tidal head in natural conditions (see Fig. 4 in GC05).

3. Results

3.1. Annual Mean Power Density

In the model-computed distribution of annual mean power density (Fig. 7) areas of high power density are confined to the southern portion of the model domain and are concentrated in channels and around headlands. Power density is highest in Cape Cod Canal, where there is significant cross-canal variation in power density marked by a decrease in power towards the channel edges. This decrease is due to frictional losses in the shallow waters along the lateral boundaries. For any given cross-section, the maximum power density occurs near the canal centerline and the magnitude is inversely correlated with the depth. The kinetic power density along the centerline is greatest at the canal's western entrance, with an annual mean value of 2.7 $\mathrm{kW\,m^{-2}}$ and maximum annual value of 16.8 $\mathrm{kW\,m^{-2}}$, and is weakest near the eastern entrance, where the annual mean value decreases to 0.5 $\mathrm{kW\,m^{-2}}$ along the stretch of canal where the width increases from 200 to 330 m. The ratio of maximum instantaneous kinetic power density to annual mean kinetic power density is approximately 5.8 throughout the canal, with the exception of the west entrance where it reaches a value of 6.3. The inlet hydraulics near the western entrance generate a slight dominance of the ebb tide (discharge from the canal).

The site with the next largest annual mean kinetic power density, with a peak value of 2.35 $\mathrm{kW\,m^{-2}}$, is Nantucket Shoals to the southwest of Nantucket Island. The power density exceeds 1.0 $\mathrm{kW\,m^{-2}}$ over a roughly 1 $\mathrm{km^2}$ patch situated 2 km from the coast. The water depth over this patch, which is in the vicinity of Old Man Shoal as marked on NOAA charts, ranges from 3 to 10 m. The strong tidal flows in Nantucket Shoals are well known to mariners, as are the hazards posed by the region's constantly shifting and shoaling bars. From an analysis of momentum balance of the barotropic tidal flow, [3] found that the nonlinear advection terms become significant in the vicinity of the Shoals, and attributed this to a large local increase in the bed stress. The relationship of kinetic power density to bathymetric features subject to morphodynamic evolution make this area a poor candidate for power extraction using fixed devices. For this reason, we chose not to examine the power potential of this area further. We also chose to exclude other areas in which high P_A ($> 1.0\ \mathrm{kW\,m^{-2}}$) is coupled with unstable bedforms from further analysis. These include a region known as Shovelfull Shoal off Monomoy Point in Chatham and Wasque Shoal off of Chappaquiddick Island, Martha's Vineyard, and Middle Ground in Vineyard Sound.

Among the Elizabeth Island channels, Woods Hole has the highest annual mean power density, which peaks at 2.13 $\mathrm{kW\,m^{-2}}$ in an area known as the Strait where the passage is most narrow. The annual power density exceeds 0.7 $\mathrm{kW\,m^{-2}}$ in a swath of water approximately 0.3 $\mathrm{km^2}$. The ratio of the maximum instantaneous to annual mean kinetic power density in the vicinity of this enhanced power patch is 5.5. Further south, Robinson Hole has a peak annual mean kinetic power density of 0.9 $\mathrm{kW\,m^{-2}}$. The area of the hole over which the kinetic power density exceeds 0.7 $\mathrm{kW\,m^{-2}}$ is very small, approximately 200 m on a side. Still further south, Quicks Hole has a peak annual mean kinetic power density of only 0.5 $\mathrm{kW\,m^{-2}}$.

Flow in Muskeget Channel has a peak annual mean power density of 1.73 $\mathrm{kW\,m^{-2}}$ and peak instantaneous annual maximum of 9.2 $\mathrm{kW\,m^{-2}}$. The ratio of maximum to annual mean power density ranges from 5.25 in the eastern side of the channel, as defined by the 15-m isobath, to 6.5 on the western side where the flow is strongly ebb dominant (see Section 3.2). Annual mean power densities in excess of 0.8 $\mathrm{kW\,m^{-2}}$ appear within an area extending approximately 2500 m in the along channel direction and 800 m in width. The area enclosed by 1.0 $\mathrm{kW\,m^{-2}}$ power threshold is roughly 50% smaller, stretching ∼2000 m along the channel and ∼400 m across the channel. The depth over most of the high-energy region exceeds 15 m.

3.2. Theoretical Resource Estimate

Based on the model-computed annual mean kinetic power density (§3.1) and prior work in the region [10], we chose to examine the theoretical power potential using turbine fences at five sites: Cape Cod Canal, Woods Hole, Robinson Hole, Quicks Hole, and Muskeget Channel (Fig. 1). The power potential of first four was estimated with a full fence across the respective channels. For Muskeget Channel, the power potential was determined for a partial fence spanning the channel between the 10-m isobaths. Although power density in Quicks Hole did not meet our threshold value of 0.7 $\mathrm{kW\,m^{-2}}$, the hole was included in our analysis to represent a site with modest power density but with a depth, in excess of 10 m, suitable for turbine emplacement. The theoretical resource for each site was determined individually to isolate the power potential of a given site. Several alternative experiments were also run to examine the potential for interaction among the sites. These experiments indicated that the only interaction of note was among Robinson, Quicks, and Woods Hole in the Elizabeth Islands. In comparison with the sum of their individual theoretical power, approximately 5% greater power was achieved when extraction was performed at the three sites simultaneously.

The site with the greatest theoretical tidal stream power is Muskeget Channel. Maximum extractable power from the channel is estimated to be 24.24 MW with M_2-only forcing, and only slightly greater, 24.29 MW, with forcing by all six constituents (Table 3, Fig. 8). The volumetric flow reduction through the channel at maximum power extraction is 44%, the highest of the five sites considered (Table 4). The site with the second largest theoretical tidal stream resource is the Cape Cod Canal. Estimated maximum tidal stream power through the canal is 12.61 MW with M_2-only forcing and 13.15 with six major constituents. Estimated flow reduction through the canal due to maximum power extraction is 42%. Quicks Hole and Woods Hole had similar maximum powers from M_2-only forcing, with 2.88 MW for the former and 2.85 MW for the latter. Robinson Hole had the smallest tidal stream resource, with an estimated maximum extracted power of 0.58 MW when forced by the six major constituents. The total tidal stream resource from all five sites is 43.8 MW.

3.3. Comparison with Analytical Approaches

Power predictions at the five sites using the appropriate analytical approaches resulted in a total power potential of 36.1 MW which is within 17% of the numerical model prediction (Table 3). By site, the relative differences ranged from a minimum difference of 3.4% at Robinson Hole to 21% at Quicks Hole. The prediction of the numerical model exceeded that of the analytical at three of the five sites (Cape Cod Canal, Muskeget Channel, and Quicks Hole).

4. Discussion

Comparison of the modeled profiles of tidal power density with power density profiles determined from CMIST and Muskeget Channel ADCP measurements gives reasonable confidence in the model's skill in estimating kinetic power density within high-flow environments that may be candidates for power extraction. In particular, the model very closely replicates the magnitude and spatial distribution of the measured power density in Muskeget Channel, including the ebb/flood asymmetry of the power density in the along- and across-channel directions (Fig. 6). From the overall model/measurement comparison, it appears that the model closely reproduces annual mean power density and shear within well-defined channels over which the annual mean power density is high. The notable exception is the failure of the model to reproduce the shear of the annual mean power density in Woods Hole Strait, at CMIST-11 (Fig. 5).

There are several characteristics of Woods Hole that make it a particularly challenging site for accurately modeling flow and power density. The Woods Hole passage turns by nearly 90°, and the navigation channels are bounded by steeply sloping rock ledges. Flow over this irregular and rough bathymetry can generate significant form drag and lateral turbulence, processes that are not well resolved in the terrain-following hydrostatic ocean model used in our study. At other high energy locations, such as Three Tree Point in Puget Sound, this form drag has been estimated to be an order of magnitude greater than the bottom drag [49]. The CMIST-11 velocity record has the greatest non-tidal variability ($\sim$5 $\mathrm{cm\,s^{-1}}$) of the 12 CMIST records, an indication of high level of turbulence intensity in the horizontal velocity field. Greater confidence in the model solution in Woods Hole passage would require more careful observations of the velocity field to provide a better understanding of the frictional control and associated energy losses. Frictional energy losses could be better parameterized in the model through changes in bottom roughness and/or lateral diffusivity. A second factor which may limit model fidelity in Woods Hole is the paucity of bathymetric data outside the navigation channels.

A larger-scale concern with our modeling approach is with the treatment of the open boundary conditions. The open boundaries in both the regional (MTM) and local (C^3M) model were clamped, constrained to follow elevation changes of the larger-scale model in which they were nested. This practice does not account for the possible effect of energy extraction on the boundary elevation field, and thus may exclude critical impacts of the extraction [50,51]. To examine the potential influence of clamping on the MTM model, we look at the contribution of extraction to the overall energy budget in the domain. The mean bottom dissipation rate under M_2 forcing is 3.8 GW. If the tidal stream resource from all five sites examined in this study (44 MW) was extracted simultaneously, this would represent only 1.2% of the natural bottom dissipation. To examine clamping effects on the C^3M model, we performed energy extraction experiments in the Cape Cod Canal using the larger scale MTM model and examined the influence of extraction on the sea level near the location of the C^3M open boundaries. The maximum M_2 head in the MTM model between the position of the two open boundaries in the C^3M is 1.66 m. At maximum extraction in the Cape Cod Canal in the regional MTM model, this maximum head difference is reduced by only 2.5 cm, which is 1.5% of the natural maximum head. These experiments indicate that clamping the surface elevation at the open boundary has limited effect on the outcome of the simulations.

An unexpected result of our study is the close agreement of the tidal stream resource estimations obtained by extracting energy from the modeled flows with estimates determined by the formulations of GC05 and GC07, which require considerably less computational effort than the numerical model. Applied to all five sites, the analytical predictions are within 17% of the value determined by the numerical model. This result is somewhat surprising as the analytical formulations are based on assumptions that are not directly applicable to these sites. In particular, assumption of the GC05 1-D approach that spatial variations of the flow occur only in the along-channel direction is counter to the significant vertical and cross-channel velocity shear observed in the fixed and shipboard ADCP data and in the model results (Figs. 5 and 6). Nevertheless, our finding may be taken as evidence for the utility of the GC05 and GC07 formulations in making rapid and inexpensive assessments of tidal-power potential in a given region.

Extraction of the maximum power under M_2-only forcing of 43.12 MW is associated with significant reductions in volumetric flow ranging from 36 to 44 percent. A 38% reduction in this power to 26.4MW would generate a volumetric flow reduction at a significantly smaller value of 15% (Table 4). Similar tradeoffs were found by [19] in their study of Minas Passage.

Notably our predictions of extractable power differ considerably from estimates of mean available power determined by [10] using point ADCP measurements to determine the energy flux through a given channel (see §1 and locations of ADCP measurements in Fig. 7). Their

13.3 MW estimate of mean available power within Muskeget Channel is considerably less than our predictions of maximum extractable power determined using the partial fence approach (24.3 MW) and the GC07 formulation (21.9 MW) (Table 3). Their 3.41 MW estimate of annual mean power in Cape Cod Canal is also significantly below the estimated the tidal stream resource determined by full-fence energy extraction (12.61 MW) or by GC05 (10.60 MW). This comparison reveals the potential inadequacy of flux based assessments of a tidal power resource and underscores the need to evaluate tidal power potential using high-resolution hydrodynamic modeling.

5. Summary

A pair of numerical models was setup to resolve the coastline and bathymetry at a scale appropriate for the assessment of the theoretical tidal stream resource of Massachusetts, USA. The model was validated through extensive comparison with sea surface height and both fixed and shipboard velocity measurements. The numerical model predicts a total of 44 MW available from five high energy sites. These sites were also studied using accepted analytical approaches which provided predictions that were within 21% of the numerical models at all sites. The numerical models can be used to provide initial power resource assessments for energy developers, offer guidance on placement of velocity measurements for further study of the resource, and facilitate optimization of turbine array design.

Acknowledgments

The authors would like to thank the reviewers for their valuable comments and suggestions. G. Cowles was supported by the U.S. Department of Energy through award DE-EE0002656 and the National Science Foundation through award NSF1336007. A. Hakim was supported by the MIT Sea Grant through award NA10OAR4170066 and the National Science Foundation through award NSF1336007. J. Churchill was supported by the MIT Sea Grant through award NA10OAR4170066. Computations were made on the UMass Dartmouth GPU cluster, which was acquired with support from NSF award CNS-0959382 and AFOSR DURIP award FA9550-10-1-0354.

References

[1] Moody, J. A., Butman, B., Beardsley, R. C., Brown, W. S., Daifuku, P., Irish, J. D., Mayer, D. A., Mofjeld, H. O., Petrie, B., Ramp, S., Smith, P., Wright, W. R., Atlas of Tidal Elevation and Current Observations on the Northeast American Continental Shelf and Slope, no. 1611 in Geological Survey bulletin, Department of the Interior, U.S. Geological Survey, 1984.

[2] Brown, W., A comparison of Georges Bank, Gulf of Maine and New England Shelf tidal dynamics, Journal of Physical Oceanography 14 (1984) 145–167.

[3] Chen, C., Huang, H., Beardsley, R. C., Xu, Q., Limeburner, R., Cowles, G. W., Sun, Y., Qi, J., Lin, H., Tidal dynamics in the Gulf of Maine and New England Shelf: An application of FVCOM, Journal of Geophysical Research 116 (C12) (2011) C12010, 00032.

[4] Redfield, A., Interference phenomena in the tides of the Woods Hole region., Journal of Marine Research 12 (1953) 121–140.

[5] Greenberg, D. A., A numerical model investigation of tidal phenomena in the Bay of Fundy and Gulf of Maine, Marine Geodesy 2 (2) (1979) 161–187.

[6] Beardsley, R. C., Chapman, D. C., Brink, K. H., Ramp, S. R., Schlitz, R., The Nantucket Shoals Flux Experiment (NSFE79). Part I: A Basic Description of the Current and Temperature Variability, Journal of Physical Oceanography 15 (6) (1985) 713–748.

[7] He, R., Wilkin, J. L., Barotropic tides on the southeast New England Shelf: A view from a hybrid data assimilative modeling approach, Journal of Geophysical Research: Oceans 111 (C8) (2006) 2156–2202.

[8] Signell, R., Tide and Wind-Forced Currents in Buzzards Bay, Massachusetts, M.S. Thesis, Massachusetts Institute of Technology (1987).

[9] USACE, Cape Cod Canal condition survey., Tech. Rep. 11-1154, U.S. Army Corps of Engineers, New England District, Concord, MA (2011).

[10] Hagerman, G., Bedard, R., Massachusetts Tidal In-Stream Energy Conversion (TISEC): Survey and Characterization of Potential Project Sites, Tech. Rep. EPRI - TP- 003 MA Rev 1, EPRI (2006).

[11] Defne, Z., Haas, K. A., Fritz, H. M., Jiang, L., French, S. P., Shi, X., Smith, B. T., Neary, V. S., Stewart, K. M., National geodatabase of tidal stream power resource in USA, Renewable and Sustainable Energy Reviews 16 (5) (2012) 3326–3338.

[12] Garrett, C., Cummins, P., The power potential of tidal currents in channels, Proceedings of the Royal Society of London A: Mathematical, Physical and Engineering Sciences 461 (2060) (2005) 2563–2572.

[13] Blunden, L., Bahaj, A., Tidal energy resource assessment for tidal stream generators, Proceedings of the Institution of Mechanical Engineers, Part A: Journal of Power and Energy 221 (2) (2007) 137–146.

[14] Neill, S. P., Jordan, J. R., Couch, S. J., Impact of tidal energy converter (TEC) arrays on the dynamics of headland sand banks, Renewable Energy 37 (1) (2012) 387–397.

[15] An evaluation of the U.S. Department of Energy's marine and hydrokinetic resource assessments, Tech. rep., National Academic Press (2013). doi:10.17226/18278.

[16] Yang, Z., Wang, T., Copping, A. E., Modeling tidal stream energy extraction and its effects on transport processes in a tidal channel and bay system using a three-dimensional coastal ocean model, Renewable Energy 50 (2013) 605–613.

[17] Garrett, C., Cummins, P., The efficiency of a turbine in a tidal channel, Journal of Fluid Mechanics 588 (1) (2007) 243–251.

[18] Sutherland, G., Foreman, M., Garrett, C., Tidal current energy assessment for Johnstone Strait, Vancouver Island, Journal of Power and Energy 221 (2) (2007) 147–157.

[19] Karsten, R. H., McMillan, J. M., Lickley, M. J., Haynes, R. D., Assessment of tidal current energy in the Minas Passage, Bay of Fundy, Proceedings of the Institution of Mechanical Engineers, Part A: Journal of Power and Energy 222 (5) (2008) 493–507.

[20] Draper, S., Adcock, T. A., Borthwick, A. G., Houlsby, G. T., Estimate of the tidal stream power resource of the Pentland Firth, Renewable Energy 63 (2014) 650–657.

[21] Chen, C., Liu, H., Beardsley, R. C., An Unstructured Grid, Finite-Volume, Three-Dimensional, Primitive Equations Ocean Model: Application to Coastal Ocean and Estuaries, Journal of Atmospheric and Oceanic Technology 20 (1) (2003) 159–186.

[22] Chen, C., Beardsley, R., Cowles, G., An Unstructured-Grid Finite-Volume Coastal Ocean Model (FVCOM) System, Oceanography 19 (1) (2006) 78–89, 00196.

[23] Madala, R. V., Piacseki, S. A., A semi-implicit numerical model for baroclinic oceans, Journal of Computational Physics 23 (2) (1977) 167–178.

[24] Kobayashi, M. H., Pereira, J. M., Pereira, J. C., A Conservative Finite-Volume Second-Order-Accurate Projection Method on Hybrid Unstructured Grids, Journal of Computational Physics 150 (1) (1999) 40–75.

[25] Cowles, G. W., Parallelization of the FVCOM Coastal Ocean Model, International Journal of High Performance Computing Applications 22 (2) (2008) 177–193.

[26] Karypis, G., Kumar, V., A Fast and High Quality Multilevel Scheme for Partitioning Irregular Graphs, SIAM Journal of Scientific Computing 20 (1) (1998) 359–392.

[27] Smagorinsky, J., General circulation experiments with the primitive equations, Monthly Weather Review 91 (3) (1963) 99–164.

[28] Burchard, H., Applied turbulence modelling in marine waters, Vol. 100, Springer Science & Business Media, 2002.

[29] Twomey, E. R., Signell, R. P., Construction of a 3-arcsecond digital elevation model for the Gulf of Maine, Technical Open File Report 2011-1127, U.S. Geological Survey, 2013.

[30] Eakins, B. W., Taylor, L. A., Carignan, K. S., Warnken, R. R., Lim, E., Medley, P. R., Digital elevation model of Nantucket, Massachusetts: Procedures, data sources and analysis, National Oceanic and Atmospheric Administration, National Environmental Satellite, Data, and Information Service, National Geophysical Data Center, Marine Geology and Geophysics Division, 2009.

[31] Pendleton, E. A., Denny, J. F., Danforth, W. W., Baldwin, W. E., Irwin, B. J., High-resolution swath interferometric data collected within Muskeget Channel, Massachusetts, Technical Open File Report 2012-1258, U.S. Geological Survey, 2014.

[32] Egbert, G., Svetlana, Y., Efficient Inverse Modeling of Barotropic Ocean Tides., Journal of Atmospheric and Oceanic Technology 19 (2002) 183–204.

[33] Pruessner, A., Fanelli, P., Paternostro, C., C-MIST: An automated oceanographic data processing software suite., in: Proceedings of the OCEANS 2007 Conference, 2007.

[34] LeBlanc, D. R., Guswa, J., Frimpter, M., Londquist, C., Ground-water resources of Cape Cod, Massachusetts, Hydrologic Investigation Atlas 692, U.S. Geological Survey, 1986.

[35] NOS Ocean Data Portal, 2016, (Last Accessed: 2017-04-20).
URL `https://data.noaa.gov/dataset`

[36] Black, P. G., D'Asaro, E. A., Sanford, T. B., Drennan, W. M., Zhang, J. A., French, J. R., Niiler, P. P., Terrill, E. J., Walsh, E. J., Air-Sea Exchange in Hurricanes: Synthesis of Observations from the Coupled Boundary Layer Air-Sea Transfer Experiment, Bulletin of the American Meteorological Society 88 (3) (2007) 357–374. `doi:10.1175/BAMS-88-3-357`.

[37] Dickey, T. D., Williams, A. J., Interdisciplinary ocean process studies on the New England Shelf, Journal of Geophysical Research: Oceans 106 (C5) (2001) 9427–9434.

[38] Howes, B., Samimy, R., Schlezinger, D., Bartlett, M., Benson, J., Marine renewable energy survey of Muskeget Channel, Technical Report Prepared for The Massachusetts Technology Collaborative, UMass Dartmouth, 2009.

[39] Pawlowicz, R., Beardsley, B., Lentz, S., Classical tidal harmonic analysis including error estimates in MATLAB using T_TIDE, Computers & Geosciences 28 (8) (2002) 929–937.

[40] Willmott, C. J., On the validation of models, Physical Geography 2 (2) (1981) 184–194.

[41] Defne, Z., Haas, K. A., Fritz, H. M., GIS based multi-criteria assessment of tidal stream power potential: A case study for Georgia, USA, Renewable and Sustainable Energy Reviews 15 (5) (2011) 2310–2321.

[42] Polagye, B., Copping, A., Kirkendall, K., Boehlert, G., Walker, S., Wainstein, M., Van Cleve, B., Environmental effects of tidal energy development: a scientific workshop, University of Washington, Seattle, WA, USA, NMFS F/SPO-116, NOAA.

[43] Bedard, R., Previsic, M., Polagye, B., Hagerman, G., Casavant, A., North America tidal in-stream energy conversion technology feasibility study, EPRI Report TP008.

[44] Myers, L., Bahaj, A., Simulated electrical power potential harnessed by marine current turbine arrays in the Alderney Race, Renewable Energy 30 (11) (2005) 1713–1731. doi:10.1016/j.renene.2005.02.008.

[45] Roc, T., Conley, D. C., Greaves, D., Methodology for tidal turbine representation in ocean circulation model, Renewable Energy 51 (2013) 448–464.

[46] Hakim, A. R., Cowles, G. W., Churchill, J. H., The Impact of Tidal Stream Turbines on Circulation and Sediment Transport in Muskeget Channel, MA, Marine Technology Society Journal 47 (4) (2013) 1–18.

[47] Karsten, R., An Assessment of the Potential of Tidal Power from Minas Passage, Bay of Fundy, using three-dimensional models, in: Proceedings of the ASME 2011 30th International Conference on Ocean, Offshore and Arctic Engineering, Rotterdam, Netherlands, 2011.

[48] Betz, A., Das Maximum der theoretisch möglichen Ausnützung des Windes durch Windmotoren, Zeitschrift für das gesamte Turbinenwesen 26 (8) (1920) 307–309.

[49] Edwards, K. A., MacCready, P., Moum, J. N., Pawlak, G., Klymak, J. M., Perlin, A., Form Drag and Mixing Due to Tidal Flow past a Sharp Point, Journal of Physical Oceanography 34 (6) (2004) 1297–1312.

[50] Garrett, C., Greenberg, D., Predicting changes in tidal regime: The open boundary problem, Journal of Physical Oceanography 7 (2) (1977) 171–181.

[51] Hasegawa, D., Sheng, J., Greenberg, D., Thompson, K., Far-field effects of tidal energy extraction in the Minas Passage on tidal circulation in the Bay of Fundy and Gulf of Maine using a nested-grid coastal circulation model, Ocean Dynamics 61 (11) (2011) 1845–1868.

699 # FIGURES

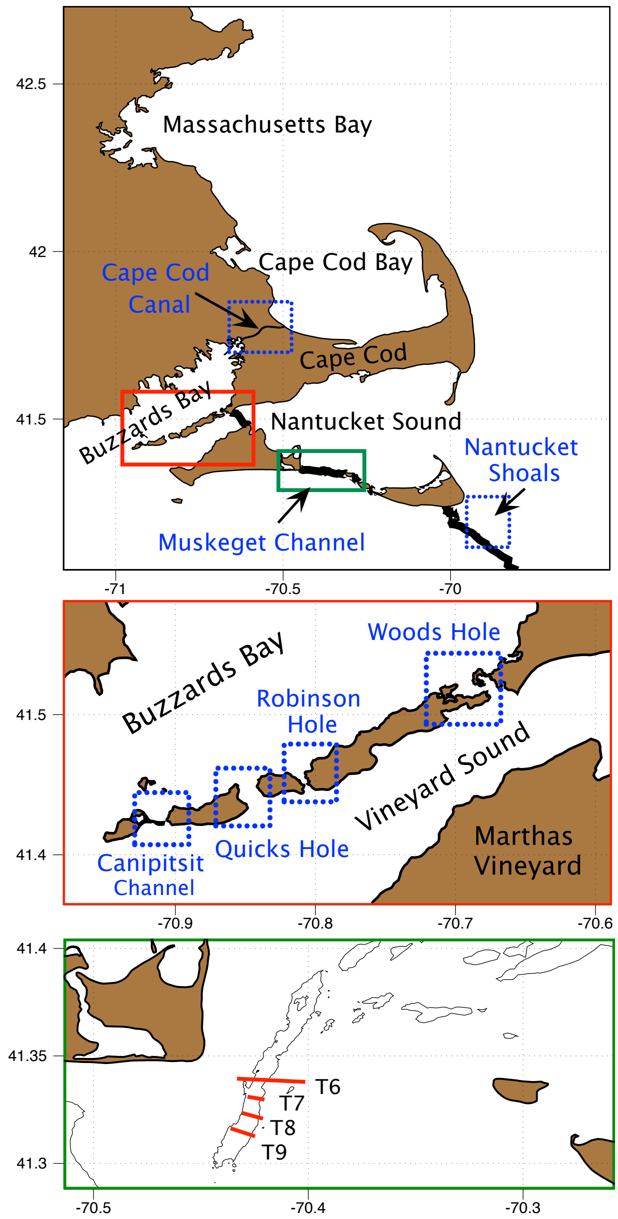

Figure 1: Upper: Coastal waters of Massachusetts with notable areas of tidal resource (boxes) and demarcation of zone of rapidly varying tidal phase (thick black line). Center: Holes and Channels separating Buzzards Bay from Vineyard Sound (see red box in upper panel for location). Lower: Muskeget Channel region with 15-m isobath and location of ADCP transects T6-T9. (see green box in upper panel for location).

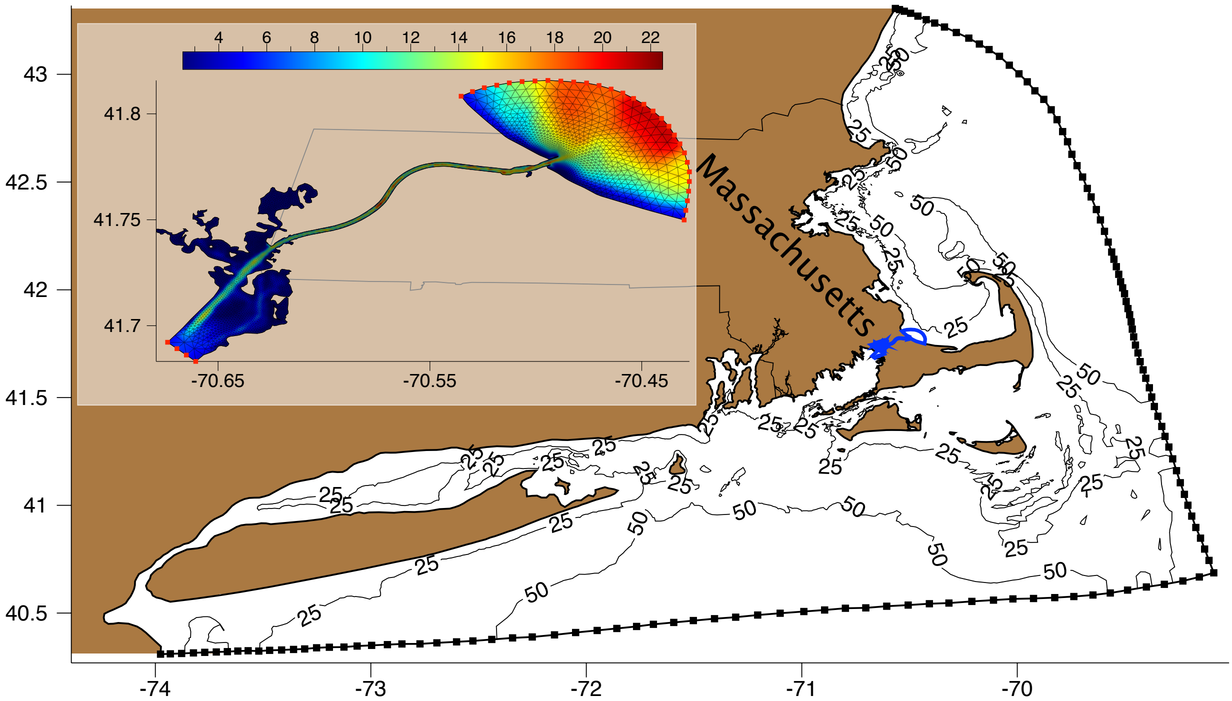

Figure 2: Main: Mass Tidal Model (MTM) domain with Massachusetts state border, 25- and 50-m isobaths, open boundary nodes (black squares), and location of C^{3}M local domain (blue outline). Inset: Cape Cod Canal Model (C^{3}M) domain and bathymetry (m) with open boundary nodes (red boxes).

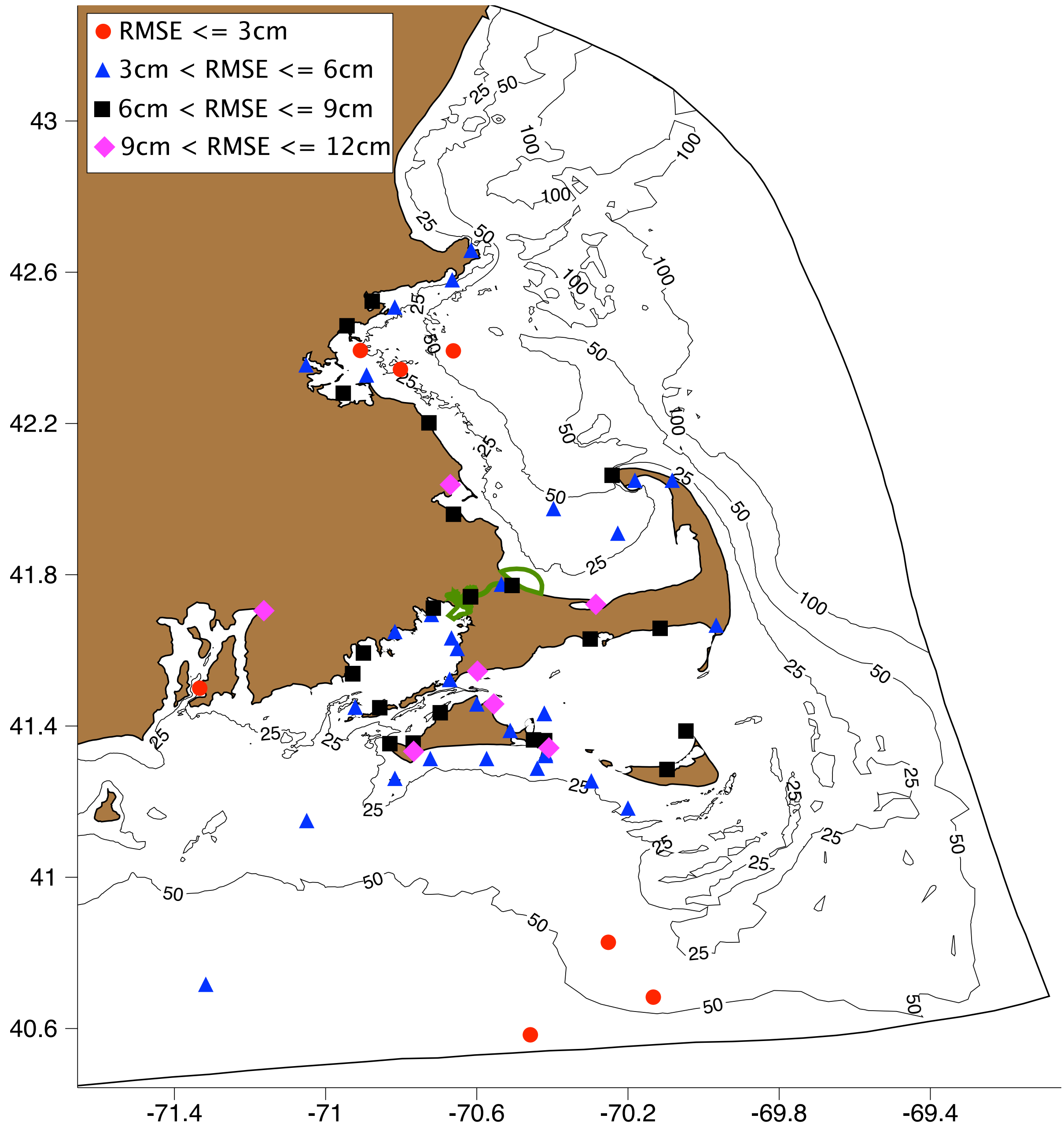

Figure 3: RMSE bins for model-computed and observed annual time series of sea surface elevation reconstructed from tidal harmonics at 73 locations in the MTM model domain and C^3M local model domain (green outline). The 25, 50, and 100 m isobaths are included for reference.

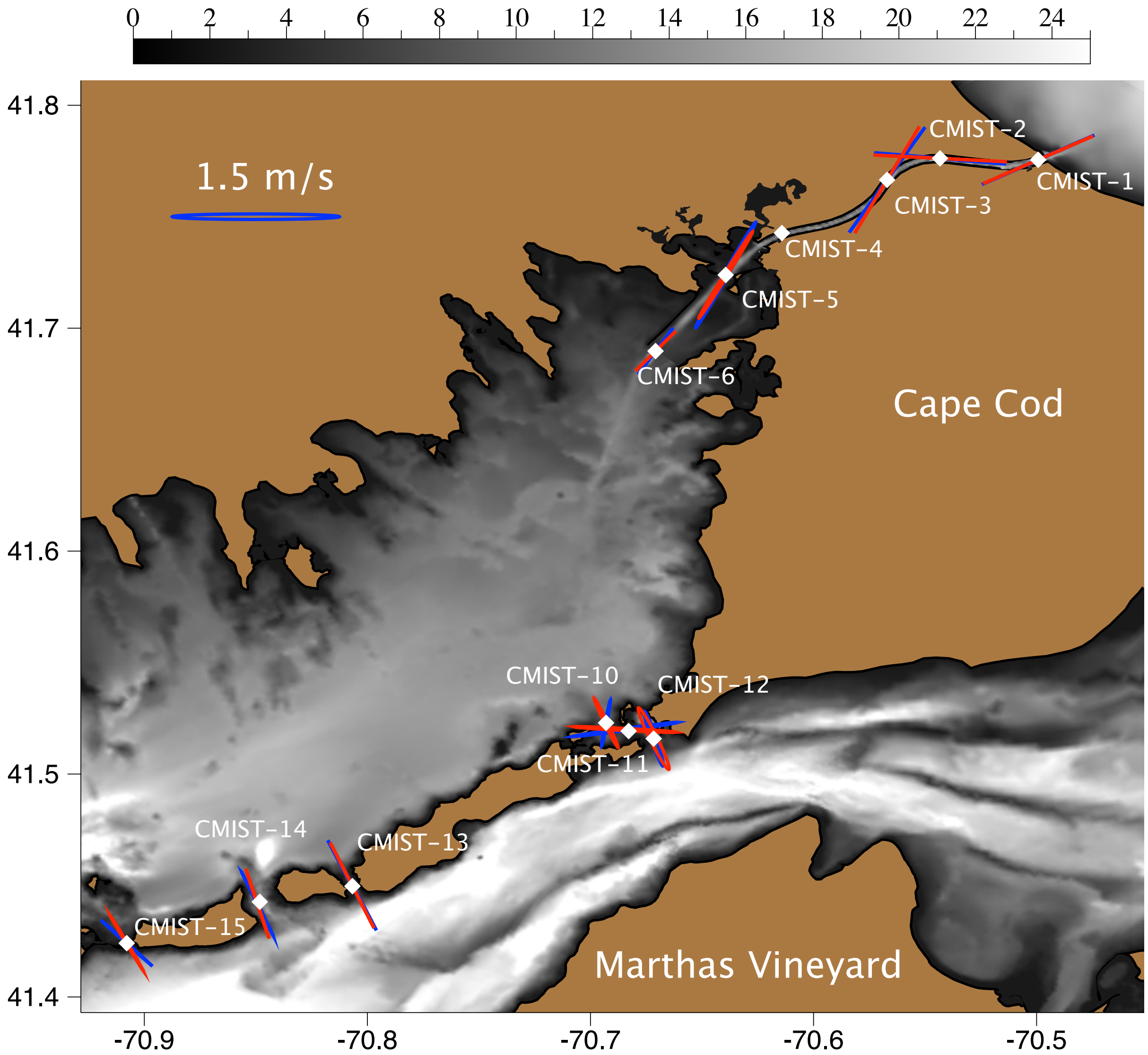

Figure 4: Tidal ellipses of model-computed (red) and observed (blue) vertically averaged velocity at 12 CMIST stations. Bathymetry [m] shown for reference. No data is plotted at CMIST-4, which is a horizontal ADCP station.

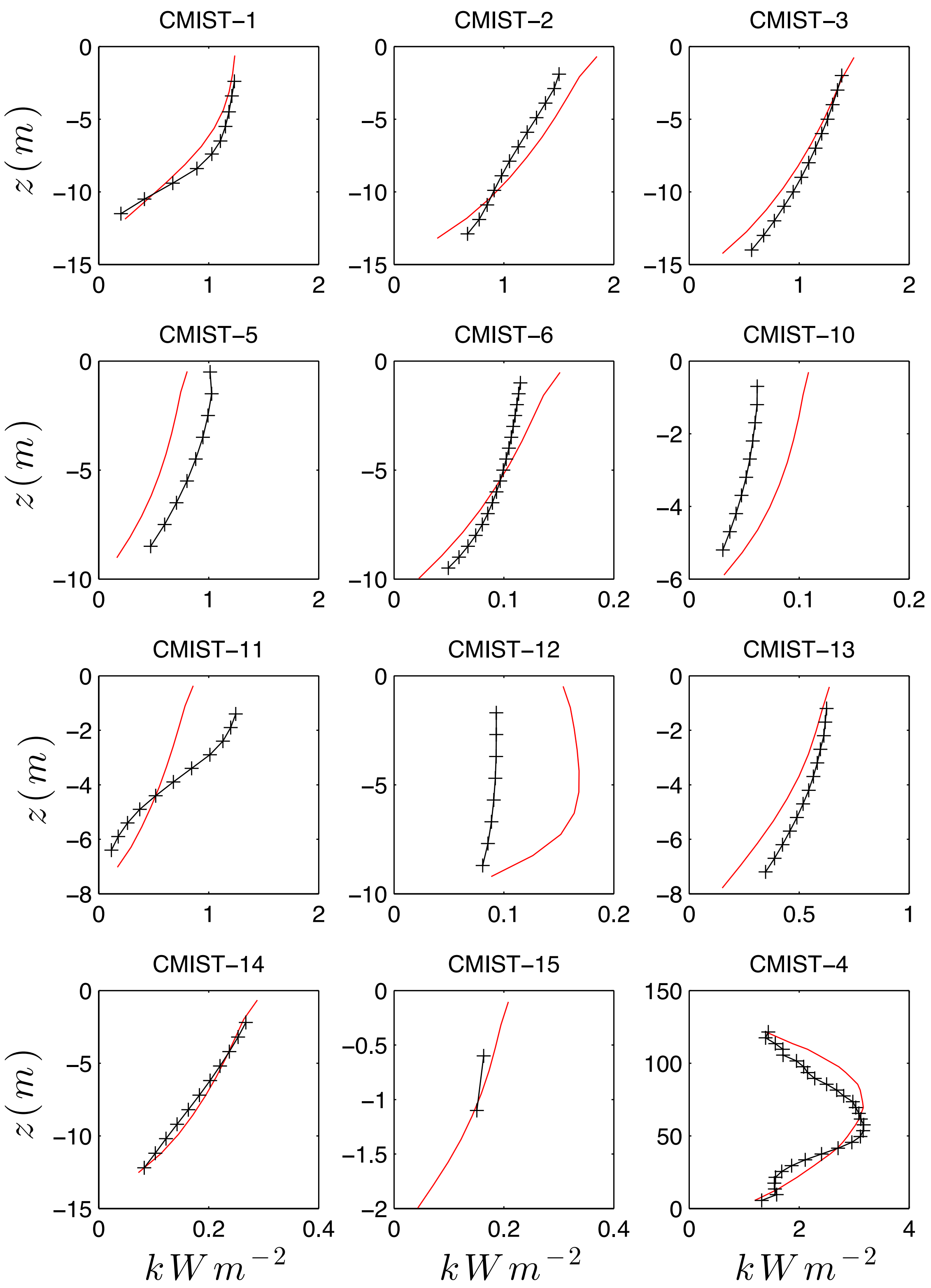

Figure 5: Profiles of model-computed (red solid line) and observed (black line with + symbols) annual mean power density at CMIST ADCP locations. All ADCPs are upward-looking with vertical axis as vertical coordinate (m) with the exception of CMIST-4 which is sideward-looking with vertical axis as horizontal distance (m). See Fig. 4 for station locations.

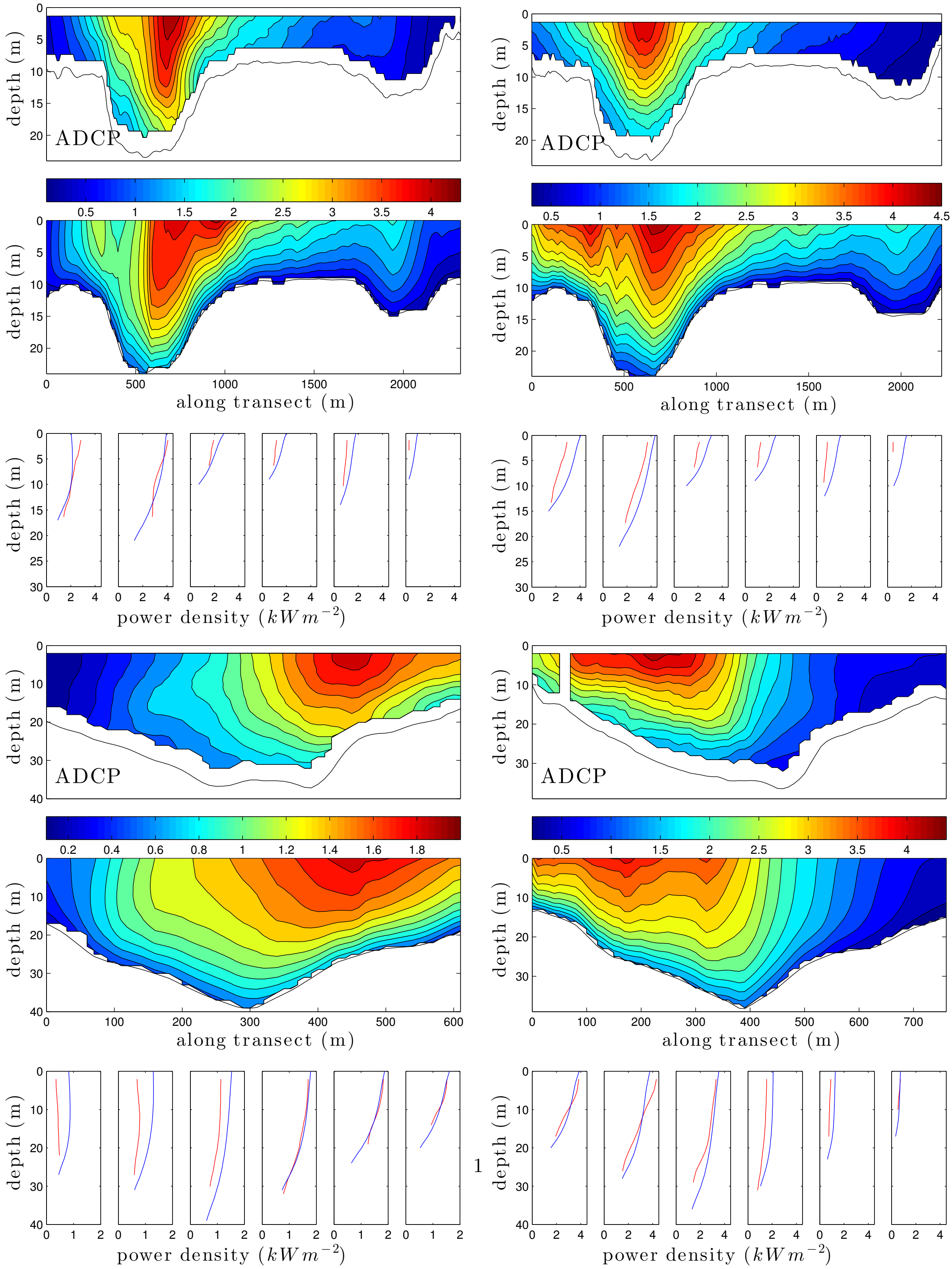

Figure 6: Comparison of model-computed and measured (ADCP) transects of power density at transect 6 (upper) and transect 8 (lower) for flood (left) and ebb (right) at Muskeget Channel. Note the different range in color axis used for flood/ebb. See Figure 1, lower panel, for transect locations. Vertical profiles of measured (red line) and model-computed (blue line) power density along each transect are shown in the lower section of each panel. Panels are oriented from west (left) to east (right).

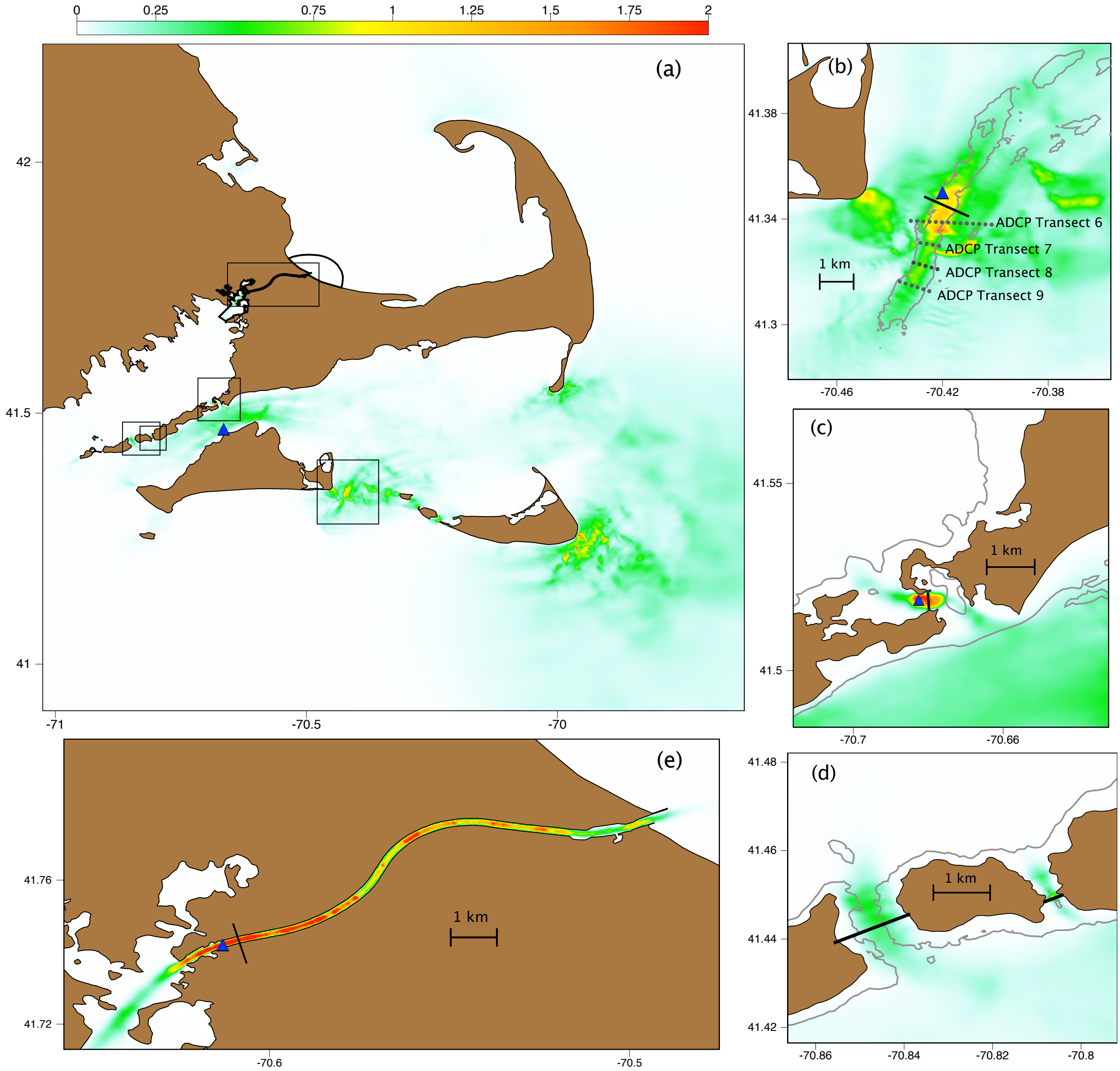

Figure 7: Annual mean vertically averaged kinetic power density P_A [kW m^{-2}] computed using the MTM and C^{3}M models. Clockwise from upper left: (a) southeastern Massachusetts region of MTM domain with C^{3}M boundary (black line) shown for reference, (b) Muskeget Channel with 15-m isobath. (c) Woods Hole with 10-m isobath (d) Robinson Hole (right) and Quicks Hole (left) with 10-m isobath, (e) Cape Cod Canal. Position of the turbine fence used for theoretical power estimation (black lines) and position of the ADCP observations used for the EPRI, 2006 assessment ([10], blue triangles) are shown for reference

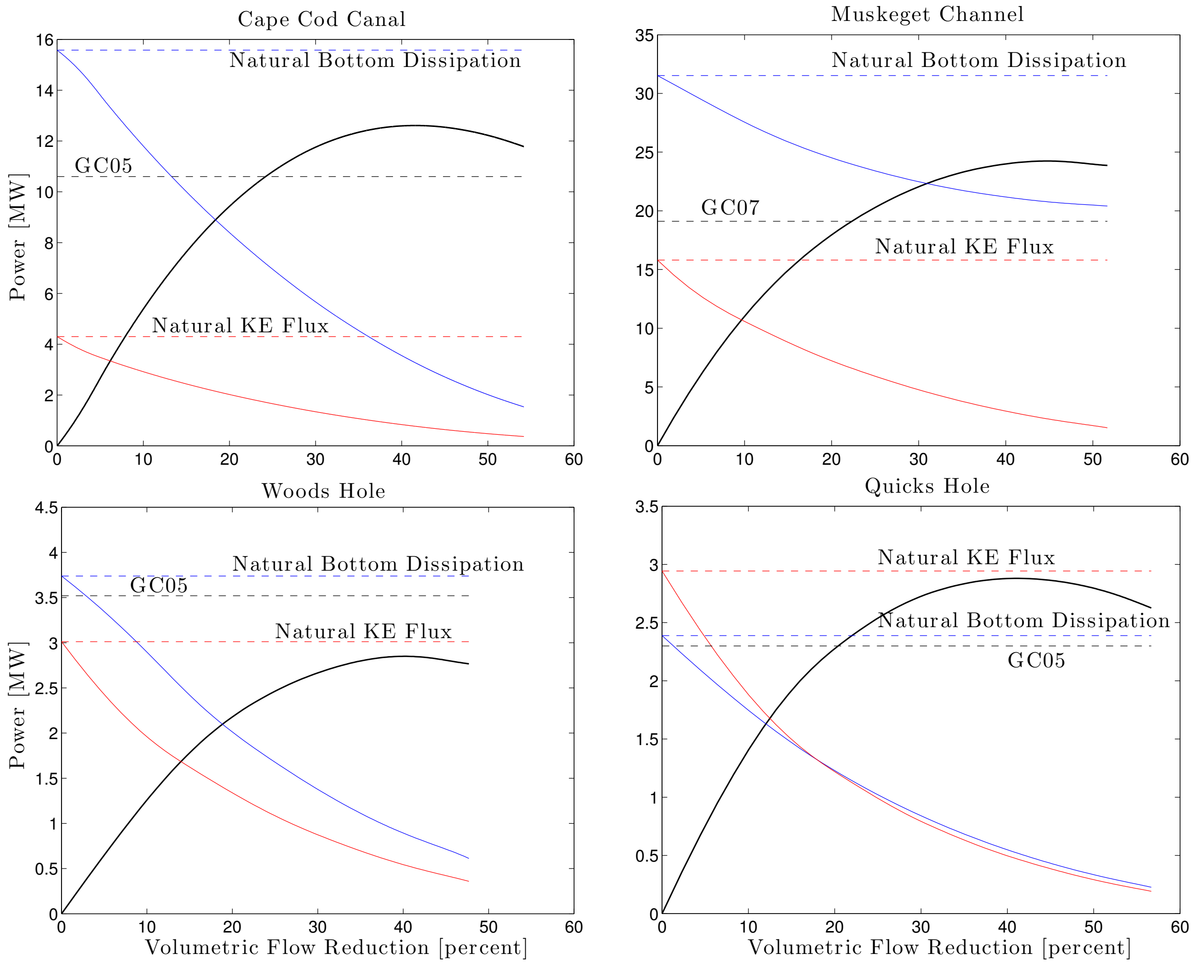

Figure 8: Tidal power components (MW) at four sites compared against percent volume flux reduction. Theoretical tidal stream power resource (black solid line), bottom dissipation (blue solid line), and kinetic energy flux (red solid line). The natural kinetic energy flux (red dashed line) and natural bottom dissipation (blue dashed line), as well as the value of the analytical estimate appropriate for the site (GC05 for full fence, GC07 for partial fence) are included for reference.

TABLES

Table 1: Skill assessment for the power density computed from an annual time series constructed using the major axis of the constituents of the vertically averaged velocity field at 11 upward looking CMIST stations within the model domains.

CMIST Station No.	Location	Willmott [-]	RMSE [$kW\,m^{-2}$]	Mean observed [$kW\,m^{-2}$]	Mean modeled [$kW\,m^{-2}$]
CMIST-01	Cape Cod Canal, East End	0.99	0.14	0.84	0.80
CMIST-02	Cape Cod Canal, Sagamore Bridge	0.99	0.19	1.08	1.11
CMIST-03	Cape Cod Canal, Bournedale	0.98	0.26	1.02	0.90
CMIST-05	Hog Neck	0.89	0.48	0.81	0.49
CMIST-06	Abiels Ledge	0.97	0.03	0.09	0.08
CMIST-10	Woods Hole, North End	0.93	0.04	0.05	0.07
CMIST-11	Woods Hole, The Strait	0.97	0.21	0.58	0.49
CMIST-12	Juniper Point	0.89	0.09	0.09	0.15
CMIST-13	Robinsons Hole	0.94	0.25	0.51	0.41
CMIST-14	Quicks Hole, Middle	0.98	0.05	0.17	0.18
CMIST-15	Canapitsit Channel	0.92	0.09	0.16	0.13

Table 2: Skill assessment for model-computed and observed power density for transects 6-9 in Muskeget Channel (Fig. 7) . RMSE and Willmott scores are computed using observed and computed values for power density interpolated to the discrete transect grid. Values for total tidal stream power (kW) through the transects are compared in columns 5-7.

Transect	Direction	RMSE $[kWm^{-2}]$	Willmott [-]	Observed Power $[kW]$	Model Power $[kW]$	Power Diff [Percent]
6	flood	0.29	0.98	40729	44416	9.00
6	ebb	0.51	0.93	40430	49417	22.00
7	flood	0.18	0.98	25367	24100	-5.00
7	ebb	0.72	0.92	37953	47730	25.00
8	flood	0.20	0.94	14046	16132	14.00
8	ebb	0.28	0.98	30297	32955	8.00
9	flood	0.08	0.97	7117	7276	2.00
9	ebb	0.31	0.96	26435	29609	12.00

Table 3: Statistics for the theoretical tidal stream resource at the five sites of interest as well as the total. A_c is the effective cross sectional area of the site and r_b is the blockage ratio. $\overline{Q}$ is the mean natural discharge, Q_o is the maximum mean natural discharge, $\overline{KE_{flux}}$ is the mean natural kinetic energy flux, a is the maximum head under M_2 forcing, and γ is the bottom friction parameter in the GC05 model. P_{GC} is the resource estimate using the appropriate Garrett and Cummins approach. $P_{MAX_{M_2}}$ is the maximum model-computed extractable power (theoretical tidal stream resource) under M_2 forcing and P_{MAX_6} is the tidal stream resource under forcing from the six major tidal constituents.

	Cape Cod Canal	Muskeget	Woods Hole	Quicks Hole	Robinsons Hole	Total
$A_c[\times 10^3 m^2]$	1.9	28.3	2.1	10.4	1.4	44.1
r_b [-]	1	0.3	1	1	1	
$\overline{Q}$ [m^3/s]	2841	24782	2674	6908	1136	38341
Q_0 [m^3/s]	4055	37988	4072	10420	1873	58408
$\overline{KE_{flux}}$ [MW]	4.30	15.8	3.01	2.94	0.56	26.61
a [m]	1.30	0.58	0.42	0.11	0.16	
γ [-]	0.2	–	0.205	0.2	0.2	
P_{GC} [MW]	10.60	19.11	3.52	2.30	0.60	36.14
$P_{MAX_{M_2}}$[MW]	12.61	24.24	2.85	2.88	0.54	43.12
P_{MAX_6}[MW]	13.15	24.29	2.90	2.92	0.58	43.84

Table 4: Volumetric reduction under various levels of power extraction for the five sites of interest. Column 2: Maximum power extraction under M_2 conditions and associated volumetric flux reduction (column 3). Power extraction for three volumetric flow reductions (columns 4-6).

			Vol. Flow Reduct.		
	$P_{max_{M_2}}$	VFR	5%	15%	25%
Cape Cod Canal	12.61	42%	2.67	7.64	10.79
Muskeget Channel	24.24	44%	6.32	14.69	20.29
Woods Hole	2.85	40%	0.58	1.75	2.46
Quicks Hole	2.88	40.1%	0.67	1.89	2.53
Robinson Hole	0.54	36%	0.24	0.39	0.49

	M_2				S_2				N_2				K_1				O_1				M_4		
	Obs		*Model*		*Obs*		*Model*		*Obs*		*Model*		*Obs*		*Model*		*Obs*		*Model*		*Obs*		*Mod*
	$A(m)$	$^\circ G$	$A(m)$	$^\circ G$	$A(m)$	$^\circ G$	$A(m)$	$^\circ G$	$A(m)$	$^\circ G$	$A(m)$	$^\circ G$	$A(m)$	$^\circ G$	$A(m)$	$^\circ G$	$A(m)$	$^\circ G$	$A(m)$	$^\circ G$	$A(m)$	$^\circ G$	$A(m)$
Nantucket Harbor	0.44	135	0.42	121	0.05	167	0.04	149	0.11	103	0.11	96	0.09	222	0.09	211	0.08	217	0.09	211	0.03	26	0.04
Great Point, Nantucket Island	0.45	127	0.45	118	0.07	164	0.05	145	0.10	96	0.11	90	0.05	214	0.09	208	0.04	196	0.09	206	0.01	12	0.03
Gay Head	0.43	11	0.42	1	0.09	35	0.09	17	0.10	355	0.09	340	0.05	172	0.07	180	0.04	206	0.05	202	0.04	14	0.03
Wasque Point	0.16	79	0.15	81	0.03	105	0.02	46	0.04	61	0.05	62	0.02	207	0.08	200	0.02	239	0.07	208	0.01	128	0.03
Oak Bluffs	0.25	115	0.22	88	0.04	151	0.03	65	0.06	84	0.06	66	0.03	207	0.08	201	0.02	190	0.07	208	0.02	327	0.05
Cedar Tree Neck	0.32	26	0.33	15	0.07	50	0.07	25	0.08	9	0.08	356	0.04	179	0.08	185	0.03	214	0.06	202	0.03	18	0.04
Nomans Land	0.44	2	0.44	355	0.09	25	0.09	14	0.10	345	0.10	334	0.06	167	0.07	178	0.04	202	0.05	201	0.04	8	0.03
Round Hill Point, Buzzards Bay	0.51	11	0.48	4	0.11	34	0.10	23	0.12	355	0.11	343	0.06	171	0.07	182	0.05	206	0.05	205	0.05	49	0.05
Clarks Point	0.53	11	0.49	5	0.11	34	0.11	24	0.13	355	0.11	344	0.07	172	0.08	182	0.05	206	0.05	206	0.05	49	0.05
Mattapoisett	0.57	10	0.52	7	0.12	33	0.11	25	0.13	354	0.12	346	0.07	170	0.08	182	0.06	204	0.06	205	0.06	46	0.06
Piney Point, Buzzards Bay	0.58	7	0.53	8	0.13	30	0.11	27	0.14	351	0.12	347	0.07	170	0.08	183	0.06	205	0.06	205	0.06	46	0.06
Cape Cod Canal, RR. Bridge	0.52	50	0.47	58	0.10	66	0.07	70	0.14	29	0.12	34	0.08	185	0.09	191	0.07	196	0.07	197	0.09	66	0.07
Chappaquoit	0.57	6	0.52	5	0.12	28	0.11	24	0.14	350	0.12	345	0.07	169	0.08	182	0.06	203	0.06	205	0.06	42	0.06
Woods Hole	0.24	35	0.26	25	0.06	36	0.06	28	0.08	20	0.07	8	0.07	189	0.08	191	0.07	205	0.06	205	0.05	355	0.05
Quicks Hole	0.51	359	0.43	1	0.11	21	0.09	19	0.12	343	0.10	341	0.06	165	0.07	182	0.05	200	0.06	204	0.05	29	0.03
Penikese Island	0.50	355	0.48	1	0.11	17	0.10	20	0.12	339	0.11	340	0.06	162	0.07	180	0.05	198	0.05	204	0.05	20	0.04
Falmouth Heights	0.20	104	0.17	74	0.03	141	0.03	43	0.04	73	0.05	54	0.02	202	0.08	200	0.02	185	0.07	208	0.00	49	0.05
Hyannis Port	0.45	132	0.40	129	0.07	170	0.04	155	0.10	101	0.10	97	0.05	217	0.09	210	0.04	199	0.09	209	0.02	8	0.06
Dennisport	0.50	134	0.51	128	0.08	172	0.05	158	0.11	103	0.13	97	0.05	218	0.10	210	0.04	199	0.09	207	0.02	16	0.05
Barnstable Harbor	1.40	120	1.39	113	0.21	157	0.21	151	0.31	89	0.31	85	0.14	210	0.14	211	0.12	193	0.11	195	0.04	112	0.03
Cape Cod Canal, east entrance	1.28	109	1.22	106	0.18	146	0.19	142	0.27	78	0.28	76	0.12	209	0.13	205	0.10	194	0.11	191	0.02	14	0.05
Plymouth, Cape Cod Bay	1.44	115	1.37	113	0.22	152	0.21	152	0.32	85	0.31	86	0.15	209	0.14	211	0.12	191	0.12	195	0.04	93	0.05
Boston	1.33	109	1.36	107	0.20	146	0.21	143	0.29	79	0.31	77	0.14	204	0.14	206	0.11	187	0.11	190	0.02	20	0.04
Rockport, Massachusetts	1.29	106	1.28	104	0.20	142	0.20	138	0.29	75	0.29	74	0.14	203	0.14	203	0.11	184	0.11	188	0.01	5	0.03
Rockport Harbor	1.29	107	1.28	104	0.19	145	0.20	138	0.30	76	0.29	74	0.14	205	0.14	203	0.12	186	0.11	188	0.01	358	0.03
Salem Harbor	1.30	109	1.31	105	0.19	146	0.20	140	0.32	78	0.30	75	0.15	207	0.13	205	0.12	188	0.11	189	0.02	360	0.03
Lynn Harbor	1.34	110	1.33	106	0.24	152	0.21	141	0.33	79	0.30	76	0.14	208	0.14	205	0.12	186	0.11	190	0.02	29	0.04
Boston Light, MA	1.32	109	1.33	106	0.20	145	0.21	141	0.30	77	0.30	76	0.14	205	0.14	205	0.11	188	0.11	189	0.01	5	0.03
Nut Island, MA	1.36	111	1.36	108	0.21	148	0.21	144	0.31	78	0.31	78	0.14	206	0.14	206	0.12	188	0.11	191	0.02	36	0.04
Scituate Harbor	1.30	111	1.31	107	0.19	148	0.20	142	0.29	77	0.30	76	0.14	206	0.13	206	0.12	189	0.11	190	0.02	360	0.03
Provincetown	1.37	112	1.35	110	0.17	152	0.21	146	0.32	79	0.31	80	0.14	207	0.13	208	0.12	188	0.11	192	0.02	10	0.04
Duxbury Harbor	1.36	121	1.38	114	0.19	162	0.21	154	0.31	90	0.31	88	0.14	214	0.14	212	0.12	194	0.12	195	0.07	128	0.06
Cape Cod Canal Sagamore	1.11	108	1.09	104	0.17	142	0.16	139	0.27	76	0.25	75	0.13	203	0.12	204	0.10	188	0.10	192	0.04	65	0.05
Buzzards Bay	0.52	50	0.47	58	0.10	66	0.07	70	0.14	29	0.12	34	0.08	185	0.09	191	0.07	195	0.07	197	0.09	66	0.07
Great Hill	0.56	11	0.54	9	0.12	34	0.11	27	0.15	351	0.12	348	0.07	166	0.08	183	0.06	199	0.06	205	0.10	46	0.06
Fall River	0.61	9	0.54	2	0.13	32	0.12	23	0.15	354	0.12	341	0.07	169	0.08	180	0.05	201	0.05	206	0.10	65	0.04
Stage Harbor	0.56	133	0.52	127	0.06	176	0.05	157	0.14	102	0.13	96	0.10	221	0.10	210	0.09	211	0.09	207	0.03	14	0.05
Round Hill	0.50	8	0.48	4	0.18	360	0.10	23	0.13	354	0.11	343	0.05	164	0.07	182	0.06	209	0.05	205	0.06	42	0.05
Woods Hole	0.24	35	0.26	25	0.06	36	0.06	28	0.08	20	0.07	8	0.07	189	0.08	191	0.07	204	0.06	205	0.05	356	0.05
Vineyard Haven Harbor	0.21	87	0.20	74	0.03	59	0.03	49	0.07	57	0.06	56	0.07	202	0.08	199	0.07	207	0.07	207	0.05	340	0.06
Penikese Island	0.49	3	0.48	1	0.11	23	0.10	20	0.12	348	0.11	340	0.06	166	0.07	180	0.05	200	0.05	204	0.06	30	0.04

Table S1: Comparison of Observed and Modeled Tidal Harmonics: Part I/II

	M_2				S_2				N_2				K_1				O_1				M_4			
	Obs		*Model*		*Obs*		*Model*		*Obs*		*Model*		*Obs*		*Model*		*Obs*		*Model*		*Obs*		*Model*	
	$A(m)$	$^\circ G$	$A(m)$	$^\circ G$	$A(m)$	$^\circ G$	$A(m)$	$^\circ G$	$A(m)$	$^\circ G$	$A(m)$	$^\circ G$	$A(m)$	$^\circ G$	$A(m)$	$^\circ G$	$A(m)$	$^\circ G$	$A(m)$	$^\circ G$	$A(m)$	$^\circ G$	$A(m)$	$^\circ G$
Edgartown	0.27	112	0.25	100	0.02	109	0.02	84	0.09	76	0.07	76	0.08	211	0.09	205	0.07	213	0.08	210	0.07	23	0.07	1
Menemsha Harbor	0.39	14	0.41	4	0.08	34	0.09	19	0.10	359	0.09	343	0.06	174	0.07	181	0.05	201	0.05	203	0.04	25	0.04	332
Nantucket Island	0.44	135	0.42	121	0.05	167	0.04	149	0.11	103	0.11	96	0.09	222	0.09	211	0.08	216	0.09	211	0.03	26	0.04	18
Cape Cod Bay East	1.33	110	1.35	110	0.22	145	0.21	146	0.26	79	0.31	80	0.15	205	0.13	208	0.11	186	0.11	191	-99.00	-99	0.04	359
Cape Cod Bay West	1.31	109	1.33	109	0.22	145	0.21	145	0.28	79	0.30	79	0.15	203	0.13	207	0.11	183	0.11	191	-99.00	-99	0.04	355
Boston Outer Harbor 1	1.32	104	1.32	105	0.21	138	0.21	141	0.30	70	0.30	75	0.14	203	0.13	205	0.12	186	0.11	189	-99.00	-99	0.03	347
Boston Outer Harbor 2	1.31	105	1.31	106	0.20	139	0.20	141	0.30	71	0.30	76	0.14	204	0.13	205	0.11	187	0.11	190	-99.00	-99	0.03	348
Boston Outer Harbor 3	1.30	105	1.29	106	0.20	139	0.20	141	0.30	71	0.30	76	0.14	202	0.13	205	0.12	187	0.11	189	-99.00	-99	0.03	346
Marblehead	1.33	102	1.31	105	0.22	137	0.20	140	0.32	72	0.30	75	0.14	201	0.13	205	0.11	182	0.11	189	-99.00	-99	0.03	345
Gloucester	1.30	105	1.29	105	0.20	140	0.20	140	0.27	79	0.30	74	0.14	201	0.13	204	0.12	183	0.11	189	-99.00	-99	0.03	340
Provincetown	1.35	110	1.30	110	0.21	145	0.20	146	0.23	84	0.30	80	0.15	206	0.13	207	0.12	185	0.11	191	-99.00	-99	0.02	350
Cape Cod Light	1.16	113	1.16	111	-99.00	-99	0.17	147	-99.00	-99	0.26	80	-99.00	-99	0.12	207	-99.00	-99	0.11	191	-99.00	-99	0.02	340
South of Nantucket	0.32	1	0.30	2	0.08	21	0.06	16	0.09	339	0.06	347	0.06	177	0.07	185	0.06	197	0.06	202	-99.00	-99	0.03	287
Nantucket Shoals 1	0.39	356	0.38	357	0.09	18	0.07	15	0.09	340	0.07	341	0.07	173	0.08	177	0.06	190	0.06	193	-99.00	-99	0.01	289
Cleveland Ledge	0.54	8	0.53	6	0.12	32	0.11	25	0.14	351	0.12	345	0.07	168	0.08	182	0.05	204	0.06	205	-99.00	-99	0.06	351
Menemsha	0.45	5	0.40	351	0.10	24	0.08	9	0.12	356	0.08	330	0.05	176	0.07	182	0.06	195	0.05	205	-99.00	-99	0.02	315
Cox Ledge	0.44	1	0.44	355	0.10	0	0.09	15	0.10	334	0.10	334	0.07	178	0.07	178	0.05	183	0.05	200	-99.00	-99	0.02	330
Picket Ledge	0.44	349	0.45	352	0.10	0	0.09	15	0.12	317	0.10	333	0.08	167	0.08	178	0.05	182	0.05	193	-99.00	-99	0.01	338
Newport, RI	0.51	1	0.50	359	0.12	23	0.11	20	0.12	345	0.11	338	0.06	168	0.07	179	0.05	199	0.05	205	-99.00	-99	0.03	347
Muskeget Channel 1	0.28	110	0.26	106	0.02	108	0.02	97	0.08	76	0.07	79	0.10	192	0.09	205	0.09	221	0.08	209	0.06	5	0.06	360
Muskeget Channel 2	0.27	111	0.26	106	0.03	115	0.02	97	0.07	68	0.07	79	0.06	207	0.09	205	0.08	214	0.08	209	0.05	8	0.06	360
Muskeget Channel 3	0.28	114	0.26	106	0.02	138	0.02	97	0.09	66	0.07	79	0.10	213	0.09	205	0.09	215	0.08	209	0.05	11	0.06	360
Muskeget Channel 4	0.21	21	0.23	17	0.04	47	0.05	21	0.07	358	0.05	4	0.07	193	0.07	191	0.07	212	0.06	205	0.03	328	0.02	305
Muskeget Channel 5	0.32	360	0.32	360	0.09	19	0.07	14	0.08	340	0.07	343	0.04	182	0.07	185	0.06	208	0.06	204	0.02	311	0.02	299
Muskeget Channel 6	0.26	12	0.25	13	0.07	24	0.05	19	0.08	355	0.05	359	0.04	191	0.07	190	0.06	211	0.06	205	0.02	328	0.02	305
Muskeget Channel 7	0.19	82	0.17	42	0.04	54	0.04	30	0.07	46	0.04	33	0.05	204	0.08	195	0.07	219	0.07	206	0.02	3	0.01	329
Muskeget Channel 9	0.18	45	0.16	74	0.05	33	0.02	44	0.07	22	0.05	58	0.05	203	0.08	200	0.07	219	0.07	208	0.01	348	0.03	350
New England Shelf 2	0.41	352	0.42	353	0.09	18	0.07	17	0.10	335	0.08	339	0.07	174	0.08	177	0.05	185	0.06	188	-99.00	-99	0.00	300
CBLAST Site 1	0.41	350	0.39	351	0.07	33	0.08	9	0.07	352	0.08	331	0.06	172	0.07	182	0.05	200	0.05	204	-99.00	-99	0.02	315
CBLAST Site 2	0.39	353	0.37	354	0.07	35	0.08	11	0.06	354	0.08	334	0.06	174	0.07	183	0.05	201	0.06	204	-99.00	-99	0.02	310
CBLAST Site 3	0.35	356	0.33	359	0.06	37	0.07	13	0.06	358	0.07	342	0.06	179	0.07	185	0.06	200	0.06	203	-99.00	-99	0.02	300
CBLAST Site 4	0.38	355	0.38	359	0.06	37	0.07	16	0.06	354	0.07	341	0.08	176	0.08	179	0.06	190	0.05	195	-99.00	-99	0.01	295

Table S2: Comparison of Observed and Modeled Tidal Harmonics: Part II/II